ANALYSIS OF SLEEP STAGE TRANSITIONS AND NETWORK PHYSIOLOGY OF CONTROL AND SLEEP APNEA SUBJECTS

By

MOUNIKA KASARANENI

Bachelor of Technology in
Electronics and Communications Engineering
S.R.K Institute of Technology
Andhra Pradesh, India
2015

Master of Science in Computer Science
Texas A&M University-Kingsville
Kingsville, Texas
2017

Submitted to the Faculty of the
Graduate College of the
Oklahoma State University
in partial fulfillment of
the requirements for
the Degree of
DOCTOR OF PHILOSOPHY
July 2022

ANALYSIS OF SLEEP STAGE TRANSITIONS AND NETWORK PHYSIOLOGY OF CONTROL AND SLEEP APNEA SUBJECTS

Dissertation Approved:

Dr. Johnson Thomas

Dissertation Adviser

Dr. Blayne Mayfield

Dr. Christopher Crick

Dr. Bruce Benjamin

Name: MOUNIKA KASARANENI

Date of Degree: JULY 2022

Title of Study: ANALYSIS OF SLEEP STAE TRANSITIONS AND NETWORK PHYSIOLOGY OF CONTROL AND SLEEP APNEA SUBJECTS

Major Field: COMPUTER SCIENCE

Abstract:

Sleep is a naturally occurring neurological state of the human body that helps restore and regenerate physiological and mental systems. Sleep comprises of AWAKE, Non-rapid Eye Movement (NREM), and Rapid Eye Movement (REM) stages. NREM sleep consists of four sleep stages N1, N2, N3, and N4. In an ideal sleep cycle, a human subject transitions through the sleep stages in the order AWAKE -> N1 -> N2 -> N3 -> N4 -> REM. Even though sleep is a resting state of the human body, physiological systems like the central nervous system, the cardiac system, and the respiratory system are still working in their vegetative state. However, the impact of sleep pathologies like sleep apnea on sleep stage transitions and connectivity between physiological systems during sleep remains largely unknown. This research presents a four-phased methodology to identify differences in sleep stage transition patterns and connectivity between physiological systems between control and sleep apnea subjects during sleep. The analysis is performed on polysomnography and histogram data collected from the Sleep Heart Health Study (SHHS) dataset. In phase I, the frequently occurring sleep stage transition patterns in healthy and unhealthy subjects are identified using the Apriori algorithm. In phase II, we studied the coupling strength and coupling direction between time series signals of brain wave activities measured as EEG waves in the δ, θ, α, σ, β, ɣ1, and ɣ2 bands. We proposed a framework that implements the Time Delay Stability (TDS) method that identifies the coupling strength between EEG bands and the LSTM-based Granger Causality (LSTMGC) estimation method that determines the coupling direction of the identified links. The results show a high coupling strength in control subjects in all sleep stages compared to sleep apnea subjects. Most links are bidirectional in the awake stage for control and sleep apnea subjects. However, in other sleep stages, more unidirectional links are identified in sleep apnea subjects, indicating a reduced coupling between EEG bands. In phase III, we developed an LSTM-based conditional Granger causality (LSTMCGC) method to identify the indirect influences of oxygen saturation ('sao2') and nasal airflow ('airflow') on brain-heart interactions during sleep. The results indicate that during light sleep, the sao2 and airflow signals have a low influence on brain-heart interactions in sleep apnea subjects but strongly influence the control subjects. In the REM sleep stage, the sao2 and airflow signals strongly influence brain-heart interactions for sleep apnea subjects and have a low influence for control subjects. In phase IV, we developed the Change in Causation during Sleep (CCS) model to study the changes in causation between physiological systems during an 8-hour long sleep. We mainly studied the causation between heart rate ('hr') and oxygen saturation signals. The overall results indicate a high causality from sao2 to hr signals in the REM sleep stage for sleep apnea subjects. But no such association is observed for healthy subjects.

TABLE OF CONTENTS

Chapter Page

LIST OF TABLES

Table Page

LIST OF FIGURES

Figure Page

CHAPTER I

INTRODUCTION

Sleep is a naturally occurring neurological state that allows the human body to restore and regenerate all the physiological and mental systems [1]. Getting a good-quality and sufficient sleep every night is essential for maintaining good health as sleep impacts many psychological processes such as memory consolidation [2-6] and biological processes such as energy expenditure, inflammation, appetite, and glucose regulation [7-10].

The primary structural organization of normal sleep consists of AWAKE, non-rapid eye movement (NREM), and eye-movement (REM) sleep stages. The NREM is further divided into four sleep stages N1, N2, N3, and N4 [11]. Stages N1 and N2 of NREM are considered light sleep, whereas N3 and N4 are considered deep sleep. During a sleep cycle, each sleep stage has unique characteristics, including variations in eye movements, brain waves, and muscle tone. Sleep stages can be identified using electroencephalographic (EEG) recordings, which trace the electrical patterns of brain activity [12, 13]. Other than adults with specific neurological disorders and newborn babies, most individuals' sleep episodes start with the NREM N1 stage. An average individual usually spends 1 to 7 minutes in the N1 stage during the first sleep cycle, which constitutes 2-5% of total sleep. During this sleep stage, the brain activity on EEG transitions from rhythmic alpha waves to low voltage to mixed frequency waves. The alpha waves have 8 to 13 brain wave cycles per second [14].

An average individual spends approximately 10 to 25 minutes in stage N2 during initial sleep cycles, and the duration increases with every successive cycle. Stage N2 constitutes around 45-55% of total sleep. During this sleep stage, low-voltage and mixed frequency waves along with sleep spindles (large, slow waves intermingle with a brief burst of activity) and K-complexes are observed in the brain activity on EEG [15] signals. Stages N3 and N4 mainly occur during the first third of the night and are collectively considered slow-wave sleep (SWS). An average individual usually spends only a few minutes in stage N3 and around 20 to 40 minutes in stage N4 during the initial sleep cycle. Stages N3 and N4 constitutes about 3-8% and 10-15% of total sleep, respectively. The brain activity on EEG for stages N3 and N4 shows high-voltage and slow-wave activity, primarily delta waves [16]. The brain activity of REM sleep constitutes low-voltage, mixed frequency waves, theta activity, and slow alpha activity. An average individual spends around 1 to 5 minutes in the REM sleep stage during the initial sleep cycle. The duration in this stage increases as the individual successfully progresses through the sleep episodes [16]. This study's research problems mainly utilize EEG brain waves collected during sleep for analysis.

Sleep is important for strengthening and maintaining mental wellbeing for both adults and children [17-23]. Recent studies show an increased interest in studying sleep disturbances such as short sleep duration [24-26], sleep disordered breathing [27] and non-restorative sleep. The research shows that the prevalence of sleep-disordered breathing (respiratory disturbance index (RDI), apnea-hypopnea index (AHI), oxygen desaturation index (ODI) >= 5/h) is around 9.0 to 76.6% in women and 24.0 to 83.8% in men. In addition, moderate to severe sleep-disordered breathing (RDI, AHI, or ODI) is around 4.0 to 50.9% in women and 7.2 to 67.2% in men [27]. A national US poll by the National Sleep Foundation in 2009 showed that around 13% of Americans had an average sleep duration of fewer than 6 hours every night in 2001, but in 2009, this increased to 20%[28]. Recent studies on sleep research indicate an association between sleep disturbances and reported health problems[29, 30]. Sleep disturbances profoundly impacts the occurrence and development of many health variables like diabetes

[31-33], metabolic syndrome [34], obesity [35], susceptibility to cold [36], and proinflammatory cytokines [37], along with severe health disorders like depression, cancer, hypertension dementia, and cardiovascular diseases [38-42].

The current study focuses on obstructive sleep apnea, a common sleep disorder caused by sleep disordered breathing [43]. For a patient with sleep apnea, breathing repetitively stops and starts during sleep, caused due to repeated collapse of the pharyngeal airway [44, 45]. Based on a report provided by the American Academy of Sleep Medicine (AASM), the economic burden of undiagnosed sleep apnea is nearly $150B. The estimated costs include nearly $26.2 billion in vehicular accidents, $86.9 billion in reduced productivity and $6.5 billion in workplace accidents [46]. Untreated sleep apnea might lead to an increased risk of heart disease, hypertension, depression, and diabetes. Thus, it is important to understand and diagnose sleep apnea. Polysomnography is a sleep disorder diagnostic tool in sleep medicine and it is used to collect physiologic parameters during sleep [47]. During polysomnography, the brain waves, heart rate, oxygen level in blood, breathing, leg movements and eye movements during sleep are recorded. The current research focuses on utilizing some of the polysomnogram signals to study and compare the physiological network graphs for a healthy subject and sleep apnea subject during sleep.

The ideal sleep stage transitions in one sleep cycle in a healthy person has the order AWAKE -> N1 ->N2 -> N3 -> N4 -> REM [48, 49]. Most physiological activities are reduced during sleep. But some of the physiological systems controlled by the central nervous system, like the cardiac system and respiratory system, are still working in their vegetative state. Sleep pathologies like sleep apnea affect sleep stage transitions, interactions, and connectivity among these physiological systems [50, 51]. In recent years, a growing interest has emerged in accessing the interactions between brain EEG bands (δ, θ, α, σ, β, $\gamma 1$, and $\gamma 2$ frequency bands), cardiovascular sub band (High frequency and low frequency bands of ECG waves) [52] during sleep. These studies show an existence of strong coupling between

EEG bands during sleep [1, 52, 53]. However, the existence of sleep apnea might affect the coupling strength and direction of coupling between physiological systems during sleep.

Studying the effects of sleep apnea on sleep stage transitions and the coupling between different organ systems can lead to a better insight into neurocognitive mechanisms during sleep. This knowledge could lead to the development of interventions that could lessen the negative influence of sleep apnea on overall health.

This research is organized as follows: Chapter 2 provides an outline of the four phased methodology of this research. The details about the studies performed in phases I, II, III and IV are provided in chapters 4, 5, 6 and 7 respectively, where each chapter discusses the following: 1) Introduction to the problem and background work, 2) Analysis procedures and models 3) Results and 4) Discussions respective to each research problem. Details about the Sleep Heart Health Study (SHHS) data used for each phase of the research are provided in chapter 3. Chapter 8 provides a summary of the results obtained for each research problem and discusses the contributions made.

CHAPTER II

RESEARCH OVERVIEW

This chapter presents an overview of the research problem: the impact of sleep apnea on sleep stage transition and physiologic network connectivity. It contains the following subsections: a) Problem statement and b) Research methodology outline.

2.1 Problem Statement

Sleep is a naturally occurring state that helps the human body restore all the physiological systems. The ideal sleep cycle for healthy subjects follows the sleep stage transition pattern Awake-> N1 -> N2 -> N3 -> N4 -> REM. Physiological systems controlled by the central nervous system like the respiratory system and cardiac system work in their vegetative state during sleep. But sleep pathologies like sleep apnea affect sleep stage transitions, interactions and connectivity among these physiological systems, which may lead to side effects such as mood changes, cognitive deficiencies, lack of focus, drowsiness and more serious health problems like cardio-vascular disease.

The goal of this study is to investigate the effects of sleep apnea on physiologic system interactions during sleep. For subjects suffering from severe sleep apnea, during the sleep apnea episodes, oxygen saturation levels drop significantly, and breathing repeatedly stops and starts. The research problems assessed in this study include the following:

a) Does sleep apnea impact the transitions between sleep stages?
b) Does sleep apnea influence the connectivity in brain networks during sleep?
c) How does the drop in oxygen saturation levels and disordered breathing influence the brain-heart connectivity during sleep for sleep apnea subjects?
d) How does the causation between oxygen saturation on heart rate signals vary during an 8-hour long sleep in control and sleep apnea subjects?

2.2 Research Methodology Outline

This research is conducted in four phases, as shown in figure 2.1 to address the four problems mentioned in section 2.1. The list of methods applied in each phase address the research problem shown in table 2.1. In the first phase, the focus is on investigating the frequent sleep stage transition patterns in subjects with and without sleep apnea. The Apriori association rule mining algorithm is used in this phase to identify frequently occurring sleep stage transitions.

In the second phase, the research focus is on finding the intra-network connectivity between the EEG frequency bands (δ, θ, α, σ, β, ɣ1, and ɣ2) for control subjects and sleep apnea subjects. In this phase, time delay stability statistical model is used to determine the strength of the links in physiological networks, and LSTM based Granger causality estimation is used to determine the directionality of the links.

The third phase focuses on identifying the indirect causation of oxygen saturation and nasal airflow signals on brain-heart interactions during sleep. For this study, the LSTM based conditional Granger causality method is used to identify the indirect causation caused by a third signal on the brain-heart connectivity.

In the fourth phase, the Change in Causation values between heart rate and oxygen saturation signals is studied in sleep apnea and control subjects. In this phase, the Change in Causation during Sleep (CCS) model is used to compute the causal values between time-series signals for every 30sec interval.

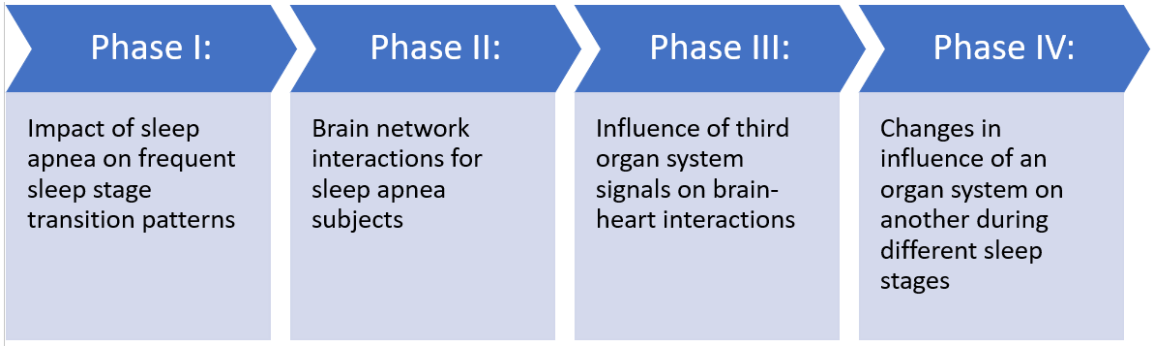

Figure 2.1: Four-phase research methodology

2.3 Contributions

In this research work, we performed apriori based sleep stage transition pattern mining and we proposed a framework which utilizes the time delay stability method to identify coupling strength and the LSTM based granger causality estimation method to identify the coupling direction of brain EEG waves in sleep apnea subjects. We developed an LSTM-based conditional Granger causality model to identify the indirect influences of sao2 and airflow signals on brain-heart interactions in control and sleep apnea subjects. We also proposed the Change in Causation during Sleep (CCS) model to identify the changes in causation values between two physiological system signals when the subject transitions from one sleep stage to another.

Table 2.1: Research Methodology Overview

Phase	Research Problems	Research Sub questions	Methods
Phase I	Impact of Sleep Apnea on sleep stage transitions	● How do sleep stage transitions occur for sleep apnea subjects?	Apriori Algorithm
Phase II	Brain network interactions for Sleep Apnea subjects	● How does the brain network interactions of healthy subjects differ from Sleep Apnea subjects?	Time Delay Stability and LSTM based Granger Causality (LSTMGC) models
Phase III	Indirect influence of third organ system signals on brain-heart interactions	● Is there any indirect influence on interactions between two physiological systems caused by a third system? ● How do the indirect influences vary between healthy and Sleep apnea subjects?	LSTM based Conditional Granger Causality (LSTMCGC) model

Phase IV	Changes in influence of an organ system on another during different sleep stages	● How does the changes in causation between two physiological systems vary through a night's sleep while transitioning between different sleep stages?	Change in Causation during Sleep (CCS) model

CHAPTER III

RESEARCH DATA

The data used for the current research is collected from the Sleep Heart Health Study (SHHS) dataset. The subsections of this chapter present the details about the SHHS data source, data used for phases 1, 2, 3, and 4, and the steps involved in data processing.

3.1 Data Source

SHHS is a multi-center cohort study database implemented by the National Heart Lung & Blood Institute [54-56] to determine the cardiovascular and other consequences of sleep-disordered breathing. This data consists of polysomnogram recordings collected over a night (average record duration is 8 hours) on participants during their visit to the participating institutions between 1995 and 1998.

3.2 Data for phase I:

The dataset for phase 1 includes polysomnography recordings of 5049 subjects who are 40 years or older with no tracheostomy, no history of treatment of Sleep Apnea, and no home oxygen therapy at the time of visit. For this study, the records with available Apnea-Hypopnea Index (AHI) and Myocardial Infarction (MI) information are only considered. AHI is a scale that can be used to determine the severity of sleep apnea. If AHI is below 5, the sleep apnea level is regarded as 1, and if the AHI level is greater than 30, then the subject is considered to have severe sleep apnea and considered level 4, as shown in table 3.1.

Table 3.1: Sleep Apnea levels based on AHI

AHI	Rating	SA Level
<5	Normal Sleep Apnea	1
5-15	Mild Sleep Apnea	2
15-30	Moderate Sleep Apnea	3
>30	Severe Sleep Apnea	4

For this study, the sleep data with details about the sleep stage (Awake, N1, N2, N3, N4, or REM) the subject in each epoch (30-sec interval) is considered. In every record, the initial few minutes of data where the subject is in the Awake stage before entering another sleep stage is trimmed because the subject might be in a wakefulness state instead of an Awake sleep stage. The sleep stages are numbered as follows: Stage 0 is Awake, stage 1 is N1, stage 2 is N2, stage 3 is N3, stage 4 is N4, and stage 5 is REM. The reduced dataset has 1775 records of subjects with sleep apnea level 1, 2036 records with level 2, 1238 records with level 3, and 762 records with level 4. The dataset is divided into three sub-datasets based on the number of MI (the records with no MI data are removed) as follows:

- Dataset 1 (SA 1, MI 0), D_1: includes records of subjects with SA level 1 and zero MI.
- Dataset 2 (SA 4, MI 0), D_2: includes records of subjects with SA level 4 and zero MI.
- Dataset 3 (SA 4, MI >= 1), D_3: includes records of subjects with SA level 4 and number of MI greater than or equal to 1.

The analysis is performed separately on each of the three data subsets, and the results are compared.

3.3 Data for phases II, III and IV

The subjects in this study included 10 control subjects and 15 subjects with Sleep Apnea. The details about the subjects considered for this study are shown in table 3.2.

Table 3.2: Description of subjects used for analysis

Variables	**Control Group**	**Sleep Apnea Group**
Hlthy25	Definitely true	Mostly false, definitely false
Age	35-45 Years	40-85 Years
During interim follow up, told by doctor that the subject has sleep apnea	No	Yes
Apnea Hypopnea Index	<2	>30
Count	5 Male, 5 Female	8 Male, 7 Female

The overnight polysomnography recording consists of the following signals [57]:

- C3/A2 and C4/A1 EEGs, sampled at 125Hz
- Right and left electrooculograms (EOGs), sampled at 50 Hz
- A bipolar submental electromyogram (EMG), sampled at 125 Hz
- HR: Heart rate derived from the ECG and sampled at 1 Hz
- Body position (using a mercury gauge sensor)
- Airflow: Detected by a nasal-oral thermocouple, sampled at 10Hz

- Oxygen saturation (saO2): These signals are sampled at 1Hz

For phase 2, only C3/A2 EEG signals are considered for analysis. Sample polysomnography recording is shown in figure 3.1. Different EEG frequency bands are extracted from the raw EEG signals for analysis and the process of extraction is explained in section 3.4.

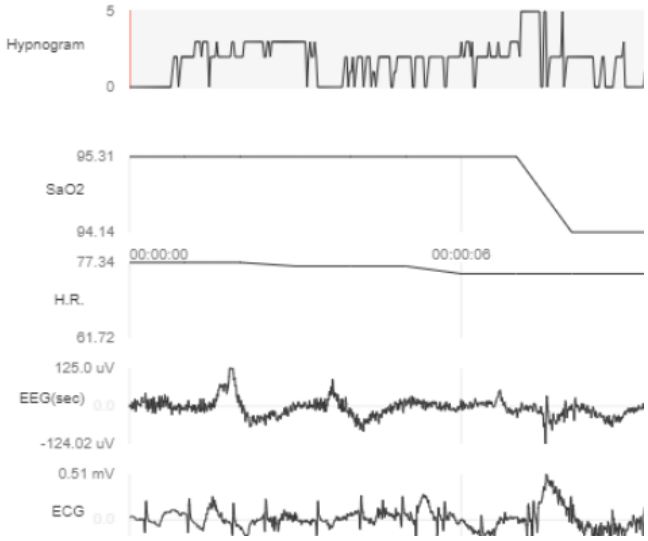

Figure 3.1: Sample polysomnography data

For phase 3, along with the EEG frequency bands, HR, sao2 and airflow signals of 10 control subjects and 15 sleep apnea subjects (table 3.2) are considered for analysis. Along with the polysomnography data, the hypnogram data (i.e., sleep stage data for every 30sec) is also considered. The airflow signals are resampled to 1 Hz frequency, such that all the signals have the same time resolution of 1 data point for every second.

For phase 4, only sao2, resampled airflow and HR signals along with hypnogram data of 10 control subjects and 15 sleep apnea subjects (table 3.2) are considered for the analysis.

3.4 EEG Signal processing:

The polysomnography data contains overall EEG signals captured at the C3/A1 brain region. The raw EEG time series signals are processed to extract frequency bands δ [0 – 4Hz], θ [4 – 8Hz], α [8 – 12Hz], σ [12 – 16Hz], β [16 – 20Hz], ɣ1 [20 – 34Hz], and ɣ2 [34 – 100Hz], which are the components of the overall EEG signal. A Fast Fourier Transform (FFT) is used to extract the different frequency bands from the raw EEG signal. In the SSHS dataset, the EEG signals are sampled at frequency 125Hz, thus there are 125 data points for each second. The raw EEG signal is divided into segments with size 60 sec with 30 sec overlap. The frequency bands are extracted for each segment using FFT and the power spectral density is calculated for each band in the 60 second window. The bands are normalized with the mean power of the entire band. The normalized bands are used for further analysis. The steps for the EEG signal processing are shown in algorithm 3.1 and the sample output of the EEG frequency band extraction is shown in figure 3.2 and figure 3.3.

The variables used in the EEG Signal Processing algorithm 3.1 are defined in table 3.3.

Table 3.3: Notations used in algorithm 3.1

Variable	**Purpose**
S	RAW EEG signal
S_{awake}	Awake stage EEG signal
S_{n12}	EEG signal in stages N1 and N2
S_{n34}	EEG signal in stages N3 and N4
S_{rem}	EEG signal in REM sleep stage
x	60 sec segment of a signal
psd	Power spectral densities of the signal

$delta_{power}$, $theta_{power}$, $alpha_{power}$, $sigma_{power}$, $beta_{power}$, $gamma1_{power}$, $gamma2_{power}$	Power of all the frequency bands
SS	Signal for a single sleep stage
power	Computed power of all the bands for a signal of size 2 sec
full_sig_power	Power of all the bands for the entire signal
nor_bands	Normalized power of all the bands for the entire signal
z_score	Computed z score of all bands

Algorithm 3.1: EEG Signal Processing

Input: Raw EEG signal *S*

Output: *nor_bands* for all sleep stages

---

1. S_{awake} = *S* where *sleep_stage* = 0
2. S_{n12} = *S* where *sleep_stage* = 1 or *sleep_stage* = 2
3. S_{n34} = *S* where *sleep_stage* = 3 or *sleep_stage* = 4
4. S_{rem} = *S* where *sleep_stage* = 5
5. **func** computePower (*x*):
6. *psd* = fft(*x*)
7. *f* = fftfreq(*x*)
8. $delta_{power}$ = *psd* [indices where 0 <= f < 3.9]
9. $theta_{power}$ = *psd* [indices where 4 <= f < 7.9]
10. $alpha_{power}$ = *psd* [indices where 8 <= f < 11.9]
11. $sigma_{power}$ = *psd* [indices where 12 <= f < 15.9]

12. $beta_{power}$ = *psd* [indices where 16 <= f < 19.9]
13. $gamma1_{power}$ = *psd* [indices where 20<= f < 33.9]
14. $gamma2_{power}$ = *psd* [indices where 34 <= f < 99.9]
15. return *power of all bands*
16. **for** each sleep stage signal *SS do*:
17. split SS into segments of 60 sec with 30 sec overlap
18. **for** each segment *i do:*
19. *power* = computePower(*i*)
20. *full_sig_power* = *full_sig_power*. append(*power*)
21. **end for**
22. *nor_bands* = z_score(*full_sig_power*)
23. **end for**

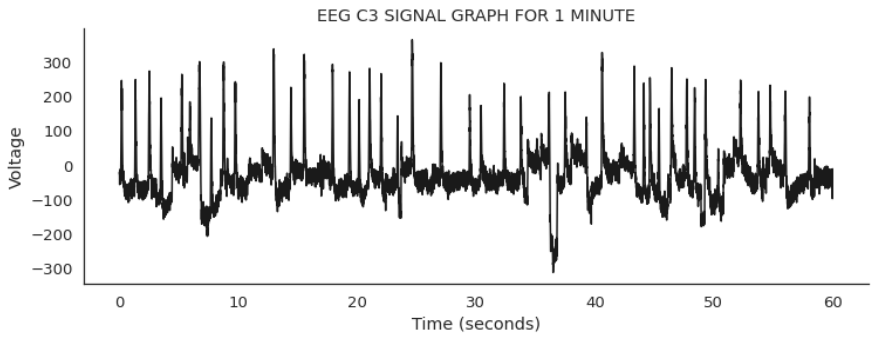

Figure 3.2. Raw EEG signal

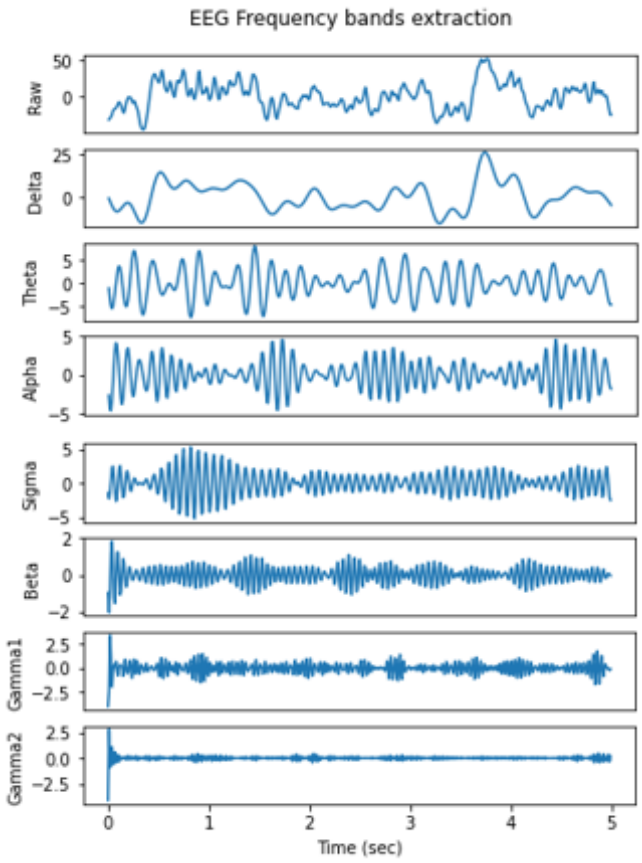

Figure 3.3: Frequency bands of EEG signal, X-axis: Time (sec), Y-axis: Power

CHAPTER IV

PHASE I: SLEEP STAGE TRANSITION ANALYSIS

This chapter discusses the frequently occurring sleep stage transition patterns of control subjects and subjects with sleep apnea or myocardial infarctions.

4.1 Introduction and Background Work

Getting continuous and sufficient sleep is necessary for physiological functions, metabolism, and long-term memories [17]. Ideally, a healthy person with normal sleep habits transitions between sleep stages in a certain pattern starting from AWAKE and alternating between Non-REM and REM sleep stages. The typical sleep architecture of a healthy young adult consists of 5 sleep stages alternating between REM and Non-REM sleep stages (N1, N2, N3, and N4) [49, 58]. The typical sleep stage pattern REM -> N1 -> N2 -> N3 -> N4 -> followed by back to REM is considered as a cycle. The duration of each sleep cycle is different with an average duration of a sleep cycle to be 90min and during a night's sleep, four to six such cycles are repeated. During the first half of sleep, stages N3 and N4 (deep sleep) are longer. But during the latter half of sleep, the duration of REM sleep gets longer alternating with stage N2 sleep [59].

A human subject needs to go through all the sleep stages because they are involved in healing and developing the body and brain. If any of the REM or Non-REM sleep stages are missing, then it would lead to the consequences of inadequate sleep on physical and mental health. Subjects with sleep disorders like sleep apnea and insomnia struggle to go through all the sleep stages. In clinical research, sleep stage transition data is used to assess sleep continuity and identify health disorders. In this study, we utilized sleep stage transition data of subjects with no sleep apnea, subjects with sleep apnea, and subjects with myocardial infarction to identify similarities and differences between frequently occurring sleep stage transition patterns among these subjects.

Christensen et al. [60] examined the transitions to REM sleep. They performed an intensive search for abnormal sleep transitions between all sleep stages and thresholds on the total number to identify specific features which can locate narcolepsy in a clinical setting. Laffan et al. [61] used the transition rates between different sleep stages as an index to measure sleep continuity. In this analysis, the transition rate is computed by calculating the total number of transitions per hour of sleep. The analysis results show that the overall and stage-specific transition rates can be used as a measure to predict sleep quality without using the traditional standards of sleep architecture. Schlemmer et al. [62] computed the probability distributions of sleep stage transitions for old and young subjects with and without a sleep disorder. The authors compared the variation in transition probabilities due to sleep disorder with the changes in transition patterns due to aging. However, the authors analyzed only one-step transition probabilities between sleep stages. Kim et al.[63] proposed a mining-based sleep pattern analysis of sleep log data collected through wearable devices. The proposed method is used to normalize the errors arising in each user's life pattern, integrate and process sleep logs, and provide a sleep index. The Apriori algorithm [64] repeatedly finds similar sequential patterns in the data to identify a final sequential pattern. The authors applied Apriori algorithm to the sleep data transitions of a user set to identify the sequential sleep patterns.

The Apriori algorithm was first proposed by Agarwal [65-68] in 1994 for association rule mining. This algorithm uses a bottom-up approach to find association rules in a database. To the best of our knowledge, frequent sleep stage transition patterns in sleep apnea subjects have not been identified before. We used the apriori-based sleep stage transition pattern mining method for the current study to analyze the frequently occurring sleep stage transition patterns in sleep apnea and myocardial infarction subjects. In this study, we considered SHHS data to analyze and identify frequently occurring sleep stage transition patterns in healthy and unhealthy subjects.

4.2 Method: Apriori algorithm-based frequent sleep stage transition pattern mining

Apriori association, a rule mining algorithm, is a well-known method to identify frequently occurring patterns in a dataset. This study exploits the Apriori algorithm to identify frequently occurring sleep stage transitions in subjects during sleep. This algorithm repeatedly searches for commonly occurring sleep stage transition patterns in the subject's sleep stage sequence. The algorithm is terminated when no more frequent sleep stage transition patterns can be found. The frequent patterns found by the algorithm satisfy the minimum support of 0.75. Support determines the pattern's frequency of occurrence. The minimum support of 0.75 indicates that frequent sleep stage transition patterns occur at least in 75% of the records.

The apriori algorithm cycles through the creation of candidate pattern set *CPk* and frequent pattern sets *FPk* of length *k* until no new candidate sets can be formed. The frequent pattern sets that satisfy the minimum threshold of 0.75 are included in the candidate pattern sets *CPk*. The frequency of occurrence of these new candidate pattern sets in the dataset is identified, and new sequential pattern sets are generated using the candidate pattern set.

The two main steps for the Apriori algorithm based frequent sleep stage transition pattern mining algorithm are explained below:

The candidate pattern set CP_1 with sequence length '*k=1*' consists of the individual sleep stages Awake, N1, N2, N3, N4 and REM.

1. The frequent pattern set FP_1 of sequence length '*k =1'* is created with sleep stages that occur in at least 75% of the records in the dataset.
2. By joining the frequent pattern sets in FP_1, candidate pattern set CP_2 with sequence length '*k=2'* is created.

The above two steps are repeated until no new candidate sets CP_{k+1} cannot be formed or frequent pattern set FP_k is not found, and the algorithm is terminated. The steps are explained below in algorithm 4.1.

The variables used in algorithm 4.1 are shown in table 4.1.

Table 4.1: Notations used in algorithm 4.1

Variable	**Purpose**
FP_k	Frequent sleep stage transition pattern set of size k, satisfying minimum support
CP_k	Candidate sleep stage transition pattern set of size k
SS	Sleep stages

Algorithm 4.1: Apriori Algorithm Based Frequent Sleep Stage Transition Pattern Mining

---

Input: Sleep stage data

Output: $FP_1 \cup FP_2 \cup FP_3 \ldots\ldots\ldots FP_k$

---

1. CP_1 : Sleep stages
2. FP_1: Sleep stages satisfying minimum support in CP_1

3. **for** (k=1; FP_k ! = Null ; k++) do begin:
4. CP_{k+1} = candidate sleep stage transition patterns generated from FP_k
5. **for** each sleep stage SS in dataset do:
6. Increase the count of all candidates in CP_{k+1} that are in *SS*
7. **end for**
8. FP_{k+1} = Candidates in C_{k+1} with minimum support
9. **end for**
10. **return** $FP_1 \cup FP_2 \cup FP_3 \ldots\ldots\ldots FP_k$

4.3 Results:

For this analysis, sleep data is divided into cycles. A cycle is considered to be from one REM state to the next REM stage. Hence, if the subject enters the REM stage 5 times in an 8-hour long sleep, the data is divided into five cycles. In this work, only the first six cycles are considered for analysis. As sleep patterns of males are different from females, they are analyzed separately.

Table 4.2 provides the details about the number of subjects that enter each cycle for males and females. The number of subjects progressing through a higher number of cycles reduces as the cycle number increases. For instance, in table 4.2, the number of subjects that enter cycle 2 with SA 1, and MI 0 is 384. But out of 384, only 378 subjects entered cycle 3. This indicates that only 378 subjects went into REM three times in their entire sleep, and six subjects were awake after they entered REM two times in their entire sleep. This indicates that the number of subjects entering REM sleep stages kept declining with the increase in the number of cycles. This trend is observed in all three datasets in both MALES and FEMALES. D_1, D_2, D_3 are different datasets as defined earlier with D_1 being healthy patients, D_2 being patients with severe sleep apnea, but no MI, and D_3 being patients with both severe sleep apnea and MI.

Table 4.2: Number of subjects entering each cycle for males and females

Cycle	MALE			FEMALE		
	D_1	**D_2**	**D_3**	**D_1**	**D_2**	**D_3**
1	391	395	37	1035	196	12
2	384	393	36	999	195	12
3	378	388	36	991	191	10
4	377	378	35	975	184	10
5	360	356	34	904	162	9
6	334	326	29	802	145	9

Cycle 1 includes the sleep stage information from the beginning of sleep till the subject enters REM for the first time. Table 4.3 provides information about the percentage of subjects that entered the N3 and N4 stages in their first sleep cycle. In dataset D_1, 84% of male subjects entered the N3 stage in their first cycle, whereas only 14% of subjects entered the N4 stage. In all the datasets, higher percentages of male and female subjects entered the N3 stage than the N4 stage in each cycle. This behavior is the expected behavior even in a healthy human being. The results also show that the more ill a patient is, the less likely he or she is to enter the 6^{th} and later sleep cycles. Over 84% of patients from D_1 subjects enter cycle 6 and 82% of D_2 subjects enter cycle 6, whereas only 78% of D_3 subjects enter cycle 6 (figure 4.1).

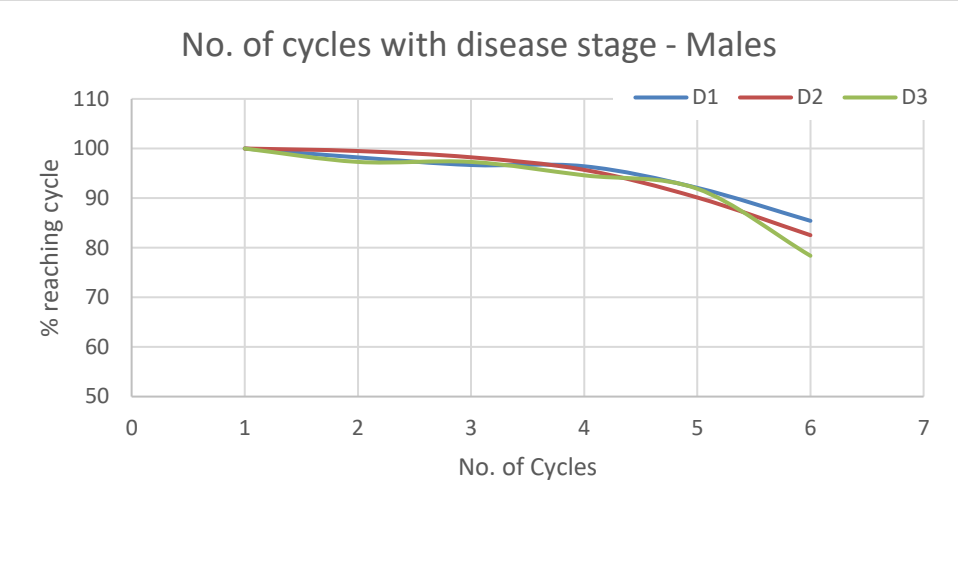

Figure 4.1: Percentage of male subjects entering each sleep cycle

Table 4.3: The number of records where N3 and N4 stages are present for Cycle 1

GENDER	D_1	D_2	D_3
MALE	N3 present in 84% of records. N4 is present in only 14% of records.	N3 present in 74% of records. N4 is present in only 12% of records.	N3 is present in 72% of records. N4 is present in only 10% of records.
FEMALE	N3 present in 93% of records. N4 present in less than 30% records.	N3 present in 93% of records. N4 is present in 26% records.	N3 is present in 91% of records. N4 is present in only 11% of records.

The following behavior is observed in higher cycles:

- A few subjects are not entering the AWAKE stage after REM. Instead, they are entering one of the N1, N2, N3, or N4 stages. The percentage of records starting from the AWAKE stage decreases as sleep apnea severity increases.
- In both males and females, the percentage of records where N3 and N4 stages are present is decreasing as sleep apnea severity is increasing or the number of MI is increasing.
- The percentages of records with N4 also reduce in the later cycles for males and females.
- The percentage of records where N3 and N4 stages are present is more in females than in males.
- The percentage of records starting with N2 increases in the later cycles for males and females.

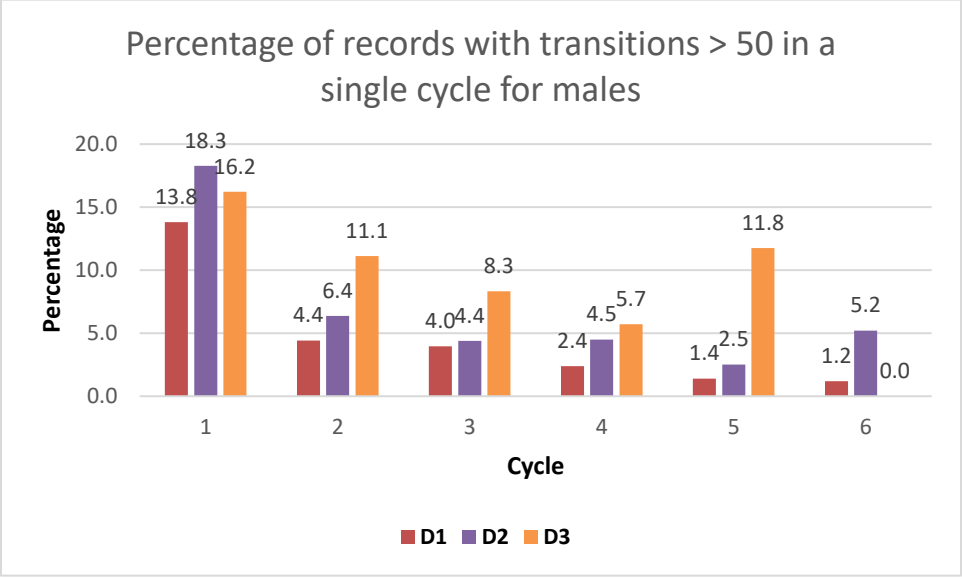

Figure 4.2: Percentage of records with more than 50 transitions in a single cycle for males subjects

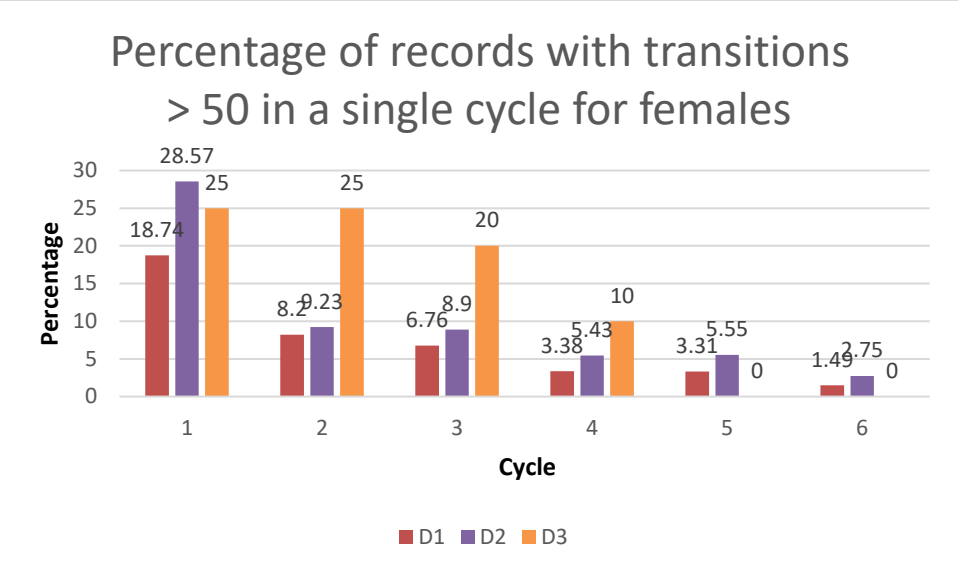

Figure 4.3: Percentage of records with more than 50 transitions in a single cycle for female subjects

Figure 4.2 and figure 4.3 include the percentages of records that have more than 50 transitions in a single cycle for males and females, respectively. Transition size is defined as the total number of sleep stage transitions that occur in a single sleep cycle. From the results in the tables, the following conclusions can be drawn:

- As Sleep Apnea severity increases, the transition size reduces, i.e., the subject is entering into REM just with fewer sleep stage transitions.
- The transition size decreases as the subjects enters more cycles.

For any given dataset, female subjects have more percentage of records with the number of transitions greater than 50.

4.3.1 Frequent sleep stage transition mining results

The Apriori algorithm is applied on datasets D_1, D_2 and D_3 separately for males and females. Each cycle is considered separately for analysis. In the analysis, the main focus is to find similar frequently occurring transition patterns among the three datasets.

The frequent transition patterns are shown as graphs in figures 4.4 and 4.5. Figure 4.4 consists of graphs for cycle 1 (i.e., Transitions from the beginning of sleep to the end of the first REM sleep). Figure 4.5 consists of the graphs for cycle 6 (i.e., sleep transitions occurring from the end of 5th REM to the end of 6th REM sleep). In these graphs, each node represents a sleep cycle where A is Awake, and R is the REM sleep stage. An edge in these graphs represents the frequent occurrence of the transition between the respective sleep stages. In figures 4.4 and 4.5, the frequently occurring transition patterns in datasets D_1 are shown as healthy, and datasets D_2 and D_3 as unhealthy.

Cycle 1:

In cycle 1, no male and female subjects (both healthy and unhealthy) entered the N4 sleep stage. The most frequently occurring transition for male and female subjects is N1 -> N2, N2 -> REM. The male healthy and unhealthy subjects are found to transition often from Awake to REM sleep stage, whereas this transition is not found frequently in female subjects. Healthy female subjects frequently transition from deep sleep to light sleep. But such frequent transition is not observed in male subjects. Unhealthy male subjects frequently transition from light sleep to REM sleep. But unhealthy female subjects transitioned to the REM stage from deep sleep stage N3. Male subjects transitioned directly from AWAKE to REM sleep frequently.

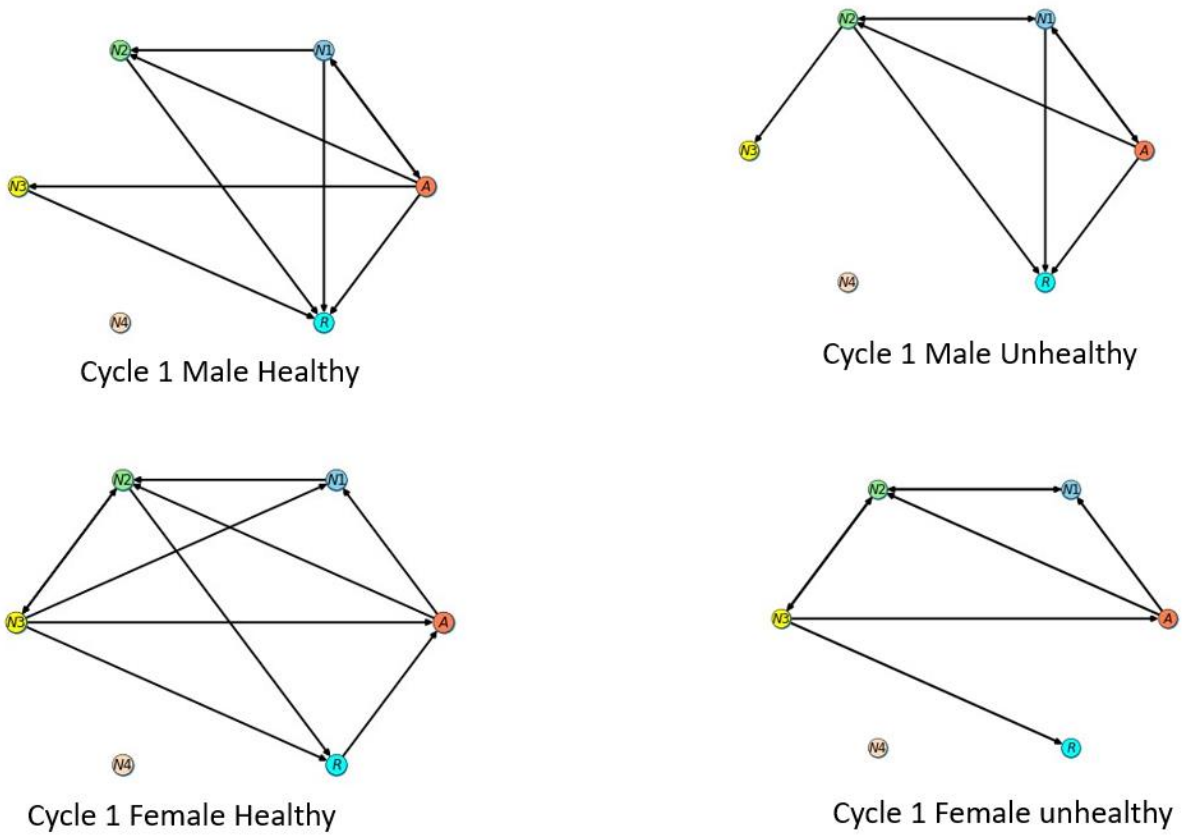

Figure 4.4: Frequent sleep stage transitions for male, female healthy and unhealthy subjects for first sleep cycle

Cycle 6:

In cycle 6, some of the frequent transition patterns in healthy and unhealthy male subjects are N1 -> N2, N2 -> REM, A -> N2, AWAKE -> R. Whereas the frequent transition patterns in female subjects are N1 -> N2, N2 -> REM, N3 -> REM. The unhealthy male and female subjects frequently transitioned from Awake to N2. Unlike females, no frequent transitions to the N3 sleep stage are found in male healthy and unhealthy subjects.

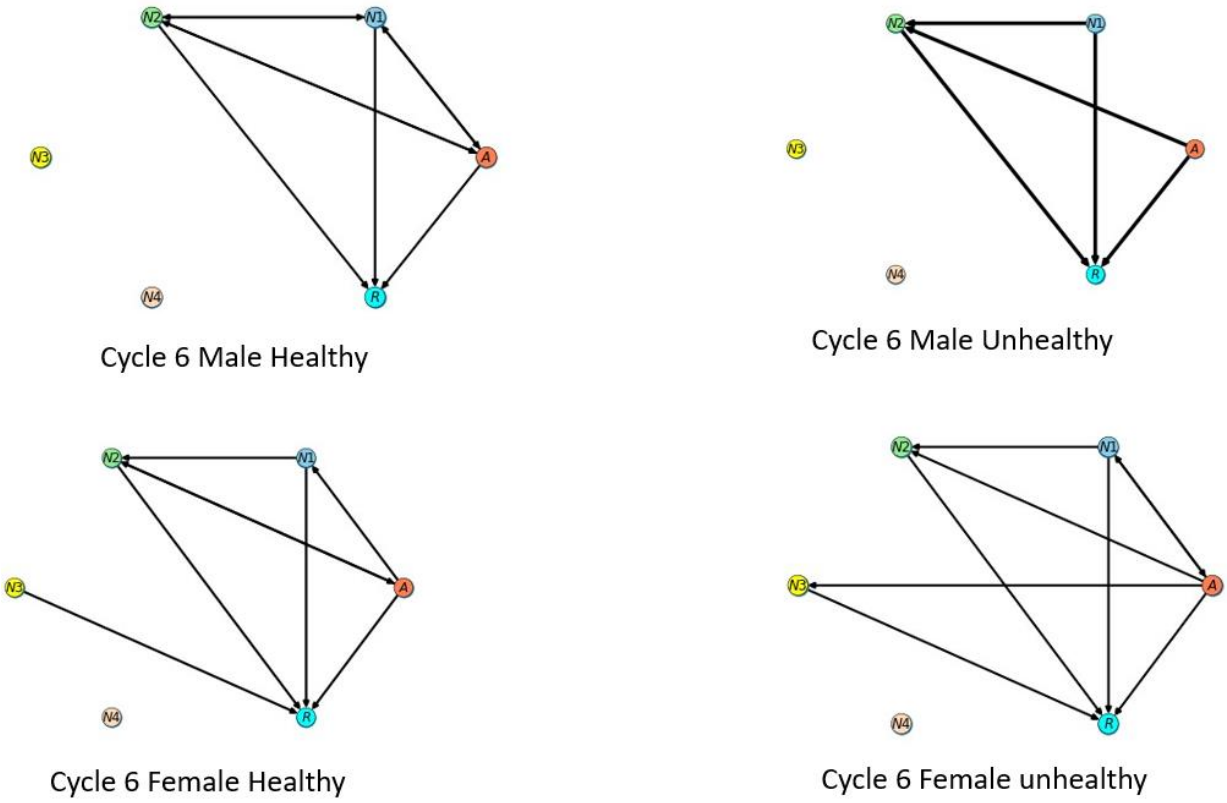

Figure 4.5: Frequent sleep stage transitions for male, female healthy and unhealthy subjects for 6th sleep cycle

The summary of results obtained are as follows:

As the severity of sleep apnea increases, the percentage of subjects with MI 1 or MI 2 or MI 3 increases. The percentage of records starting from AWAKE is reduced in the later cycles for both males and females. As Sleep Apnea severity increases, the transition size is reduced, which implies the subject is entering into REM just with few transitions. For any given dataset, female subjects have more percentage of records with sizes > 10, 50 and 100 when compared to males. The more frequently found short cycles are:

{N2;REM}, {N1;REM}, {N1;N2;REM}, {AWAKE;REM}, {AWAKE;N2;REM} , {AWAKE;N1;REM}, {AWAKE;N1;N2;REM}.

N3 and N4 are present in a greater number of records in females than males. The subjects with severe sleep apnea and the subjects with severe sleep apnea and MI 1,2 or 3 have similar patterns, but very few records of data are available to analyze for higher number of cycles. In the SA 1 MI 0 datasets many records have repetitions of the same small pattern before reaching the REM stage for both males and females; patterns like {AWAKE; N1 ; AWAKE; N1; AWAKE…..REM}.

4.4 Conclusion

Sleep helps the human body to restore and regenerate all the physiological and mental systems. Our results suggest that the sicker a person is, the fewer sleep cycles or she will go through in a typical night's sleep. The more ill a person is, the more likely the sleep cycles will be incomplete. A healthy person transitions through sleep stages AWAKE to REM in the order AWAKE, N1, N2, N3, N4, REM, and back to AWAKE. The sleep stage transitions can be utilized to determine sleep continuity and identify health disorders. In this study, we utilized sleep stage transition data to identify frequently occurring sleep stage transition patterns in subjects with sleep apnea, subjects with no sleep apnea, and subjects with myocardial infarction. The sleep stage transition analysis for subjects with sleep apnea and myocardial infarction shows that most of the time, the subjects are not transitioning through the ideal cycle (i.e., AWAKE -> N1 -> N2 -> N3 -> N4 -> REM). The frequently found sleep stage transition patterns in the subjects are {N2: REM}, {N1:REM}, {N1;N2;REM}, {AWAKE;REM}, {AWAKE;N2;REM}, {AWAKE;N1;REM}, {AWAKE;N1;N2;REM}. High frequency of these patterns indicate a sleep problem like sleep apnea.

CHAPTER V

PHASE II: INTRA BRAIN NETWORK CONNECTIVITY DURING SLEEP

This chapter discusses the intra-network coupling between brain bands (δ, θ, α, σ, β, ɣ1, and ɣ2) during sleep, which is identified using the methods TDS and LSTM based Granger causality estimation (LSTMGC).

5.1 Introduction and Background Work

Healthy sleep is essential for the human body to stave off diseases, reduce stress and strengthen and maintain long-term memories [17]. Sleep is expressed as a period of reduced activity where the blood pressure and temperature are dropped, and physiological demands are reduced. However, research over the past 60 years shows that the brain remains active during sleep and other physiological systems like the cardiovascular system and the respiratory system are still working in their vegetative state collectively as an integrated network. Recent studies demonstrate analytical models of dynamic integrated physiological networks during sleep and indicate how multiple factors like sleep pathologies affect the coupling of integrated networks [69]. The recommended sleep for adults is 7-8hrs every day. Habitually sleeping outside the normal sleep range may lead to serious health problems and sleep disorders [24-26]. Even though sleep is a resting state, most of the physiological systems like cardiac system, respiratory system and central nervous system are working in their vegetative state. Sleep pathologies like sleep apnea affect the interactions among the physiological systems, and their effects on these physiological system networks are largely unknown

Literature shows that researchers have applied the following methods to identify the integrated physiological network interactions: a) Computational methods based on time delay, b) Methods based on Transfer Entropy (TE), and c) Methods based on Granger Causality (GC). These methods utilized the overnight polysomnography (PSG) data of human subjects. The PSG data includes signals like electroencephalography (EEG), electrocardiography (ECG), electrooculography (EOG), oxygen saturation, and respiration [24].

The implementation of computational methods based on time delay to understand the interactions among different physiological systems can be found in the works developed by Bartsch et al, Ivanov et al[52, 70]. The authors developed an analytical method based on the concept of time delay stability to identify and quantify networks of physiologic interactions from long-term continuous, multi-channel physiological recordings. The authors developed a physiologically motivated visualization framework to map networks of dynamical organ interactions to graphical objects encoded with information about the coupling strength of network links quantified using the time delay stability measure. The findings of this methodology demonstrate a direct association between network topology and physiologic function and provide new insights into understanding how health and distinct physiologic states emerge from networked interactions among nonlinear multi-component complex systems. The authors found that during different physiologic states, the network of organ-to-organ interactions is characterized by different configurations of links and links strength. Overall, in sleep network physiology, the authors discussed only the link strength between physiologic network nodes but not the directionality of the links. In addition, the analysis was not performed on subjects with sleep apnea but only on healthy subjects.

Methods like directed information [71] and transfer entropy [72] are able to detect the nonlinear dependencies between past and future with minimal assumptions about the predictive relationships. But these estimators have high variance and require large amounts of data for reliable estimation. These approaches also suffer from the curse of dimensionality when the number of time series is growing [73].

For understanding the relation between two time series, among the available choices, Granger causality [74, 75] is the commonly used framework. The approaches such as lagged correlation [76] or coherence [76] analyze strictly bivariate covariance relationships between the time series but Granger causality metrics depend on the activity of the entire system of time series, thus making them more appropriate for understanding high dimensional complex data streams.

Vector autoregressive (VAR) model is a popular model which assumes linear time series dynamics to estimate Granger causality [75, 77]. In this model, the time lags of a time series have a linear effect on the future of other time series and the magnitude of the linear coefficients quantifies the Granger causal effect. However, in this model, to assess Granger causality the maximum time lag should be specified explicitly. If the lag is too short, the Granger causal connections occurring at longer time lags between series will be missed. If the lag is too larger, overfitting may occur. Hierarchical lasso [78] and truncating penalties [79] have been used to automatically select the lags while protecting against overfitting. However, this method may fail when the relation between the past of one series and future of another have nonlinear dependencies [80-82].

Neural networks are capable of representing complex nonlinear and non-additive interactions between inputs and outputs. Methods such as multilayer perceptrons (MLPs) [83-85] and recurrent

neural networks (RNNs) like long-short term memory networks (LSTM) [86] have shown improved performance in forecasting multivariate time series given their past.

Tank et al. [87, 88] proposed a class of nonlinear methods for estimation of Granger causality by applying structured multilayer perceptrons (MLPs) or recurrent neural networks (RNNs) combined with sparsity-inducing penalties on the weights on the input time series. The authors proposed component multilayer perceptron (cMLP) and component long-short term memory (cLSTM) architectures with lasso penalty to select Granger causality on the DREAM3 dataset. The provided approaches outperform the existing Granger causality approaches.

Faes et. al. [53] performed Granger causality by vector autoregressive (VAR) modeling on components of heart rate variability using time series analysis and EEG power in the δ, θ, α, σ, β bands for 10 healthy subjects during sleep. The significance of each link in the network is assessed using F-statistics. The whole-night analysis revealed the existence of a fully connected network of brain-heart and brain-brain interactions, with the β EEG power acting as a hub that conveys the largest number of GC links between the heart and brain nodes. These links became progressively weaker when assessed during light sleep, deep sleep, and REM sleep, thus suggesting that brain-heart GC networks are sustained mainly by sleep stage transitions. However, the disadvantage of using the VAR model is that the time lags of a series directly impact the future of other series. Thus, maximum time lag to be considered has to be specified explicitly when assessing GC.

Alvardo et. al. [89] analyzed the polysomnography of 28 patients diagnosed with obstructive sleep apnea (OSA) and compared the results with 10 control subjects. The authors performed Granger causality estimation on the EEG and EKG signals from the polysomnography time series to

measure the connectivity among brain waves (δ, θ, α, σ, β) and three spectral sub bands for heart rate variability of OSA patients before and during continuous positive air pressure (CPAP). Jhon et. al. [1] provided a framework to measure causality that connects central nervous system and cardiac system in people diagnosed with OSA before and during treatment with CPAP. The authors used artificial neural networks to obtain models for Granger causality computation on EKG and EEG signals recorded in polysomnographic studies. However, the analysis is performed for the whole night without considering the separate sleep stages.

To the best of our knowledge, the studies based on Granger causality estimation in sleep, performed analysis only on a whole night's sleep data without considering separate sleep stages or sleep apnea subjects' data, and the network physiology analysis performed using the time delay stability method only determined the strength of the links but not the directionality. To overcome the limitations of existing methods, and to identify the strength and directionality of the physiological network links for sleep apnea subjects, we propose a framework that incorporates both LSTM based Granger causality and the time delay stability method.

5.2 Model: Time Delay Stability (TDS)

The TDS method is used to identify the strength of the links between EEG bands δ, θ, α, σ, β, ɣ1, and ɣ2 frequency bands. The steps of the TDS method are shown in figure 5.1 and algorithm 5.1. In TDS, to find the coupling strength between two frequency bands, the two-time series are divided into segments of length 60 sec with a 30 sec overlap (line 1). Within each segment, the cross-correlation function with lag values ranging from -60 to +60 is calculated (lines 2 to 9). Time delay t_0 is the lag at which the absolute value of cross-correlation is maximum in each segment. Stable coupling between two time series corresponds to a stable time delay t_0 for multiple consequent segments. The absence of stable coupling between two time series corresponds to large fluctuations in time delay t_0. In the TDS method, if the time delay t_0 does not vary by more than +/-1 for at least 5 consecutive segments, then these segments are identified as stable. This process is repeated for the entire time series segments by using a sliding window with step size of one segment (lines 18 to 21). The percentage of time delay stability is shown in equation 1.

$$\%tds = (no.of\ stable\ segments/total\ number\ of\ segments) * 100 \quad (1)$$

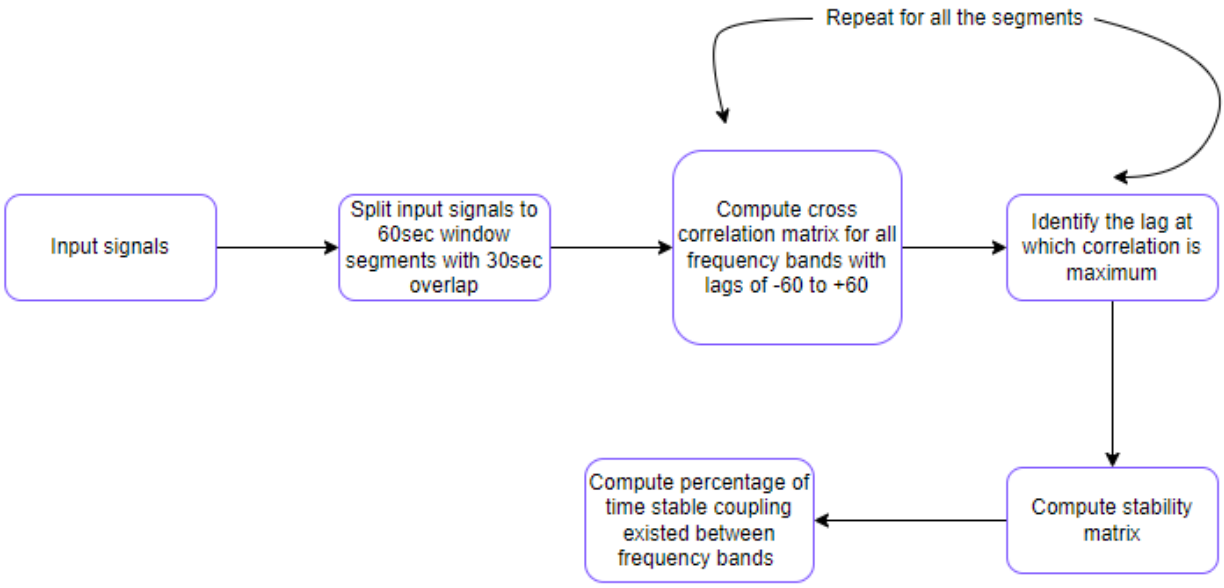

Figure 5.1: Steps in time delay stability method

The variables used in algorithm 5.1 are shown in table 5.1

Table 5.1: Notations used in algorithm 5.1

Variable	**Purpose**
X_1, X_2	Input normalized frequency band
l_{st}	Strength of link between two frequency bands
corr_val	Cross correlation value between two series at a given lag
corr_array	Array of correlation values between two series at all lags
S_{lag}	Lag at which correlation is maximum
lag_{array}	Array with all segment's lags
$diff_{array}$	Array with difference of lags for five consecutive segments
c	Count
S_{st}	Segment stability

St_{mat}	Stability matrix

Algorithm 5.1: Time Delay Stability Algorithm

Input: Series X_1 , Series X_2

Output: l_{st}

1. Split X_1 , X_2 into *v* segments
2. **for** each segment *i do*:
3. **for** each *lag* in range (-60, +60) *do*:
4. *corr_val* = cross_correlation(X_{1i}, X_{2i})
5. *corr_array* = *corr_val*.append(corr_val)
6. **end for**
7. S_{lag} = argmax(corr_array)
8. lag_{array} = lag_{array}.append(S_{lag})
9. **end for**
10. **func** segmentStability(*array*):
11. compute $diff_{array}$
12. *c* = count($diff_{array}$ < =1)
13. **if** *c* >= 4 *then*:
14. return “stable”
15. **else** *then*:
16. return “unstable”
17. **end if**
18. **for** *j* in range (0, len(lag_{max})-5) *do*:

19. S_{st} = segmentStability(lag_{max}[j,j+6])

20. St_{mat} = St_{mat}.append(S_{st})

21. **end for**

22. l_{st} = (no. of stable segments)/ (total no. of segments)

5.3 TDS Results:

The results obtained for the TDS method are shown as graphs in figure 5.2. In the graphs, each node represents a frequency subsystem and the edge between nodes indicate coupling between EEG bands. For this analysis, the links with %*tds* > 45% are only considered. The results of %*tds* are given a *score* as shown in equation 2. If the %*tds* > 80%, a score of 3 is assigned for the subject for a particular edge. For instance, if the obtained %*tds* between delta and alpha bands is 50%, then the score of 1 is given for the edge between delta and alpha.

$$score = \begin{cases} 3 & if\ \%tds > 80\% \\ 1 & if\ 45\% < \%tds < 80\% \\ 0 & if\ \%tds < 45\% \end{cases} \quad (2)$$

The overall weight of links is obtained by taking the score of all the subjects into consideration. The equation for the overall link weight is shown in equation 3. In the graphs, the thickness of the links is de termined by

$$Link\ Weight = \sum_{i=1}^{N} score_i \quad (3)$$

The thickness of the links in graphs is determined by the link weight value.

To analyze, the full night sleep data is split based on the sleep stages. Stages N1 and N2 are combined as these two stages are considered as light sleep. Stages N3 and N4 are combined as

these two stages are considered as deep sleep. Thus, the TDS method is applied to the following data groups: a) full night sleep, b) Awake, c) stages N1 and N2, d) stages N3 and N4, and e) REM.

When the full night sleep data is considered, a fully connected network between EEG bands is observed for both the control group and the sleep apnea group. However, the connectivity between EEG bands is reduced when individual sleep stages are considered. The percentages of links with stable connectivity for the control group and the sleep apnea group are shown in figure 5.3. For both the groups, a greater number of stable links are observed in the awake stage and the least number of stable links are observed in the N3 and N4 stages. The control group has a higher percentage of stable links than the sleep apnea group in every sleep stage. However, the percentage of links in the REM stage are increased when compared to the N1 & N2 and the N3 & N4 sleep stages for the control group. But they are reduced for the sleep apnea group. An overall higher average link strength is observed in the control group when compared with sleep apnea group. In the control group awake stage, links are present between α and σ, β, ɣ1, and ɣ2 bands. But, in the sleep apnea group awake stage, there are no links to the α band. A strong coupling is seen between the ɣ1 and ɣ2 bands in all sleep stages for both the control group and the sleep apnea group.

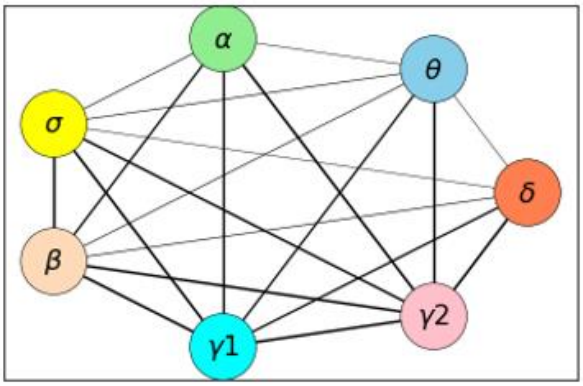

(a) Control Group : Full Night Sleep

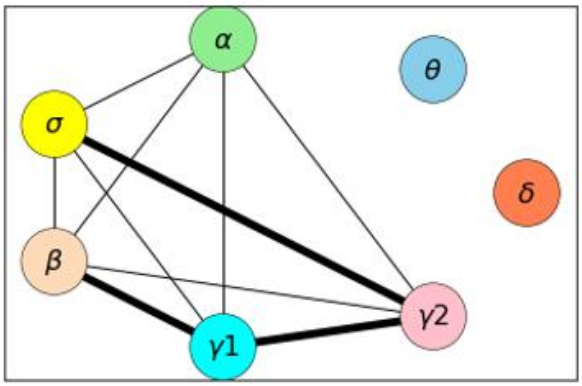

(b) Control Group : Awake stage

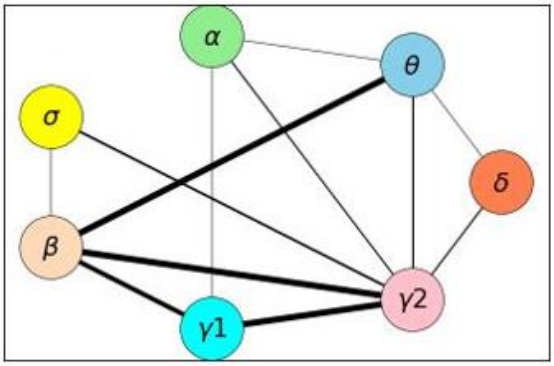

(c) Control Group : Stages N1, N2

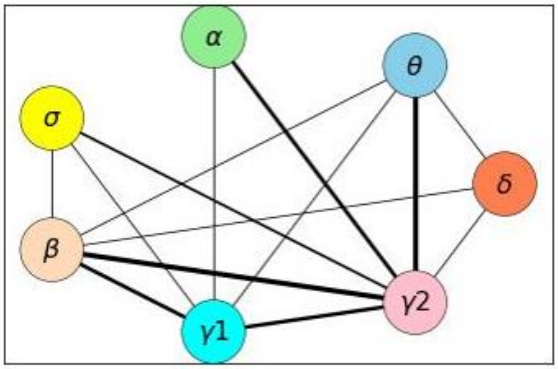

(d) Control Group : Stages N3, N4

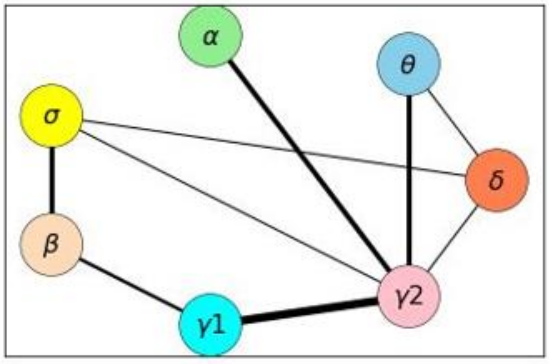

(e) Control Group : REM Stage

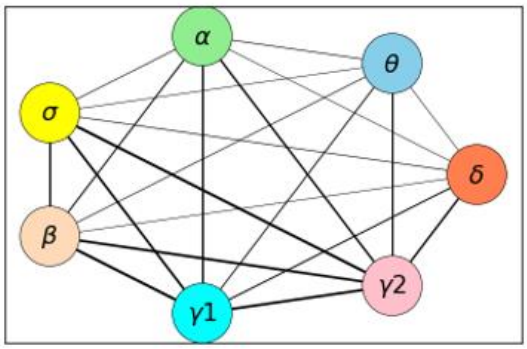

(f) Sleep Apnea Group : Full Night Sleep

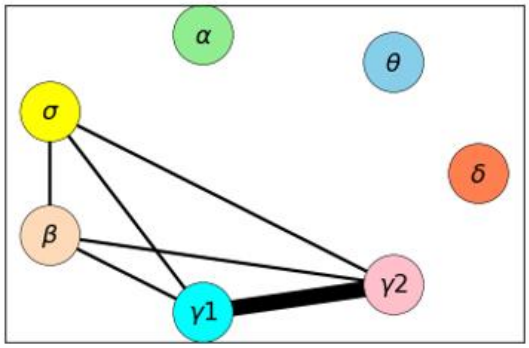

(g) Sleep Apnea Group : Awake stage

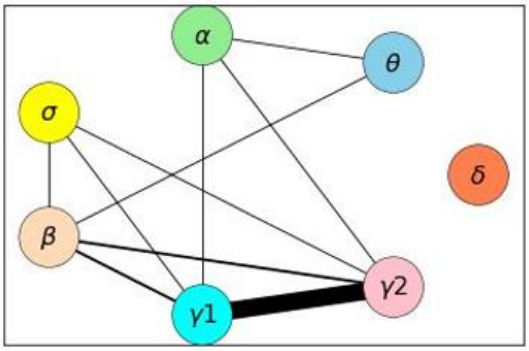

(h) Sleep Apnea Group : Stages N1,N2

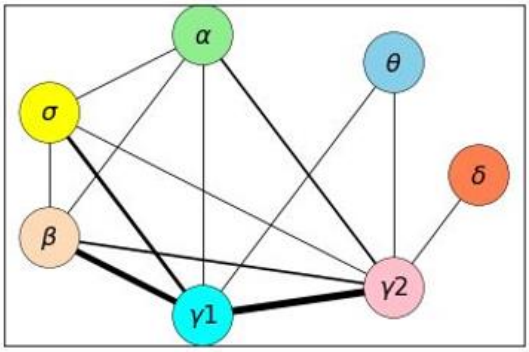

(i) Sleep Apnea Group : Stages N3, N4

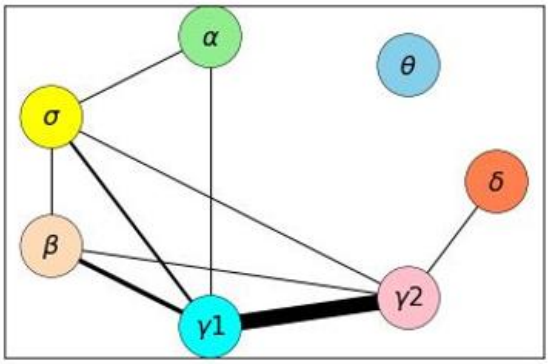

(j) Sleep Apnea Group : REM Stage

Figure 5.2 TDS method results

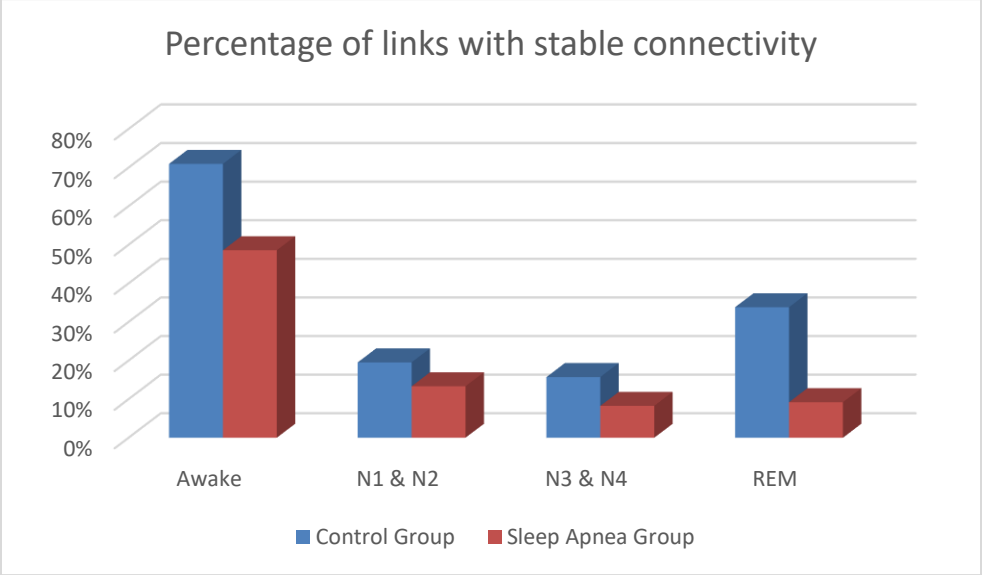

Figure 5.3: Percentage of links with stable connectivity in control group and sleep apnea group subjects

5.4 Model: LSTM based Granger Causality Estimation (LSTMGC):

The coupling direction between two EEG bands is identified using the LSTMGC method where LSTM is applied to the principle of Granger causality.

5.4.1 Granger Causality

Granger causality is a statistical hypothesis test to determine if one time series is useful in forecasting another. Time series Y is said to Granger cause series X if including the past values of series Y improves prediction of X's future values. In the original Granger causality, the causal dependence is measured using the vector autoregressive model. For instance, consider a two stochastic systems X_t and Y_t. The two systems can be mathematically represented as shown in equations (4), (5):

$$X_t = \sum_{j=1}^{p} a_1 X_{t-j} + E_1 \quad (4)$$

$$Y_t = \sum_{j=1}^{p} b_1 Y_{t-j} + E_2 \quad (5)$$

where p is the maximum number of lagged observations, E_1 and E_2 are residuals for each series, a and b are the coefficients that relate to X_t and Y_t systems. To find if series Y_t Granger causes series X_t, an unrestricted prediction model of X_t combining with Y_t is given as follows:

$$X_t = \sum_{j=1}^{p} a_2 X_{t-j} + \sum_{j=1}^{p} b_2 Y_{t-j} + E_1 \quad (6)$$

$$Causality = ln \frac{var(Error_{reduced})}{var(Error_{full})} \quad (7)$$

Where, $Error_{reduced}$ = Error of model considering only X_t.

$Error_{full}$ = Error of model considering both X_t and Y_t.

The Granger causality is the logarithm of ratio of variances of reduced error and variances of full error as shown in equation (7).

5.4.2 LSTMGC

In the LSTMGC model, to forecast the EEG frequency bands, a recurrent neural network LSTM is used. LSTM is a recurrent neural network model used for processing sequence data like time-series signals. The significance of the LSTM model is that it contains a gate mechanism to provide better performance in long-term prediction. The architecture of the LSTMGC model is shown in figure 5.4.

Using the LSTMGC model, the behavior of the studied systems can be represented as shown in equations (8) and (9).

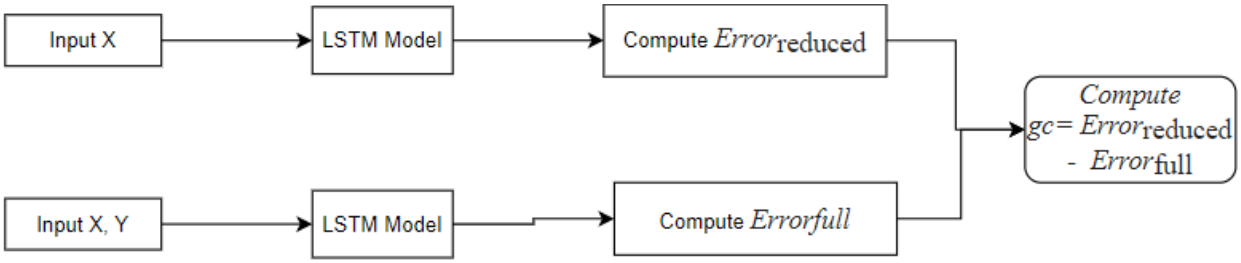

(a)

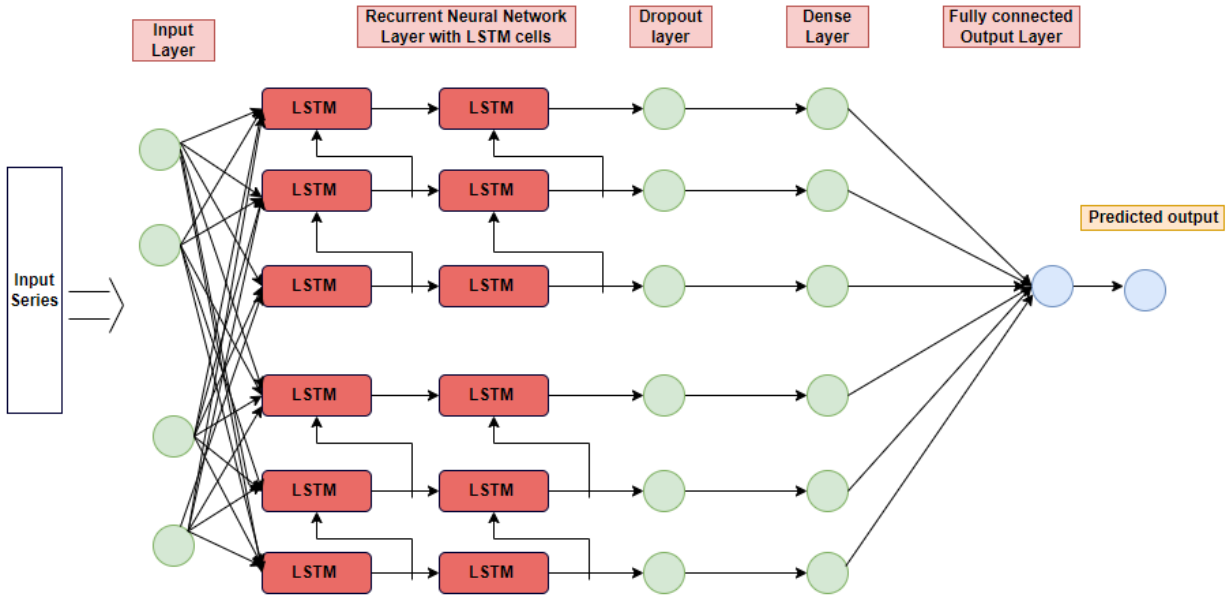

(b)

Figure 5.4: (a) LSTMGC overall architecture (b) LSTM model architecture

$$X_t = f\left(\sum_{j=1}^{p} a_1 X_{t-j} + E_1\right) \quad (8)$$

$$X_t = f\left(\sum_{j=1}^{p} a_2 X_{t-j} + \sum_{j=1}^{p} b_2 Y_{t-j} + E_1\right) \quad (9)$$

Where f is a nonlinear function, p is the maximum number of lagged observations, E_1 is the forecasting residues, a and b are the coefficients that relate to X_t and Y_t systems.

The Granger causality for LSTMGC model is measured as given in equation (10).

$$gc = Error_{reduced} - Error_{full} \tag{10}$$

where, $Error_{reduced}$ = forecasting error of model considering only X_t as input.

$Error_{full}$ = forecasting error of model considering both X_t and Y_t as input.

If the gc value is zero, then the system Y_t has no influence on system X_t. Positive gc value refers to the existence of effective connectivity between systems Y_t to X_t.

5.5 LSTMGC Results

For this study, the N1 and N2 stages' data are combined during analysis as these stages collectively belong to light sleep (LS). Similarly, N3 and N4 stage data are combined as they belong to deep sleep (DS). The coupling direction of the links that exist between the EEG bands is shown in figure 5.2. This is obtained through the LSTMGC method. The results obtained using the LSTMGC method for the control group and sleep apnea group are shown in figure 5.5. Most of the links are bidirectional in the awake stage for both the control group and the sleep apnea group. In the N1 and N2 stages for the sleep apnea group, the link between σ and ɣ2, β and ɣ1 are unidirectional, whereas it is bidirectional in the control group. Furthermore, the link between β and θ are in opposite directions in this stage for both groups. In the REM stage for the control group, there are links to θ from δ, ɣ1, and ɣ2 subsystem. However, in the REM stage for the sleep apnea group there are no links to the θ subsystem. Furthermore, the links between β, ɣ2 and α, ɣ1 in the REM stage for sleep apnea subjects are present according to the TDS method results. But the gc value obtained for both these links is negative. Thus, TDS indicates a correlation, but not necessarily a link. There is thus no link present between these bands in the LSTMGC results. Overall, bidirectional links are seen

for both control and sleep apnea subjects in the AWAKE sleep stage. But, for other sleep stages, unidirectional links are identified in sleep apnea subjects.

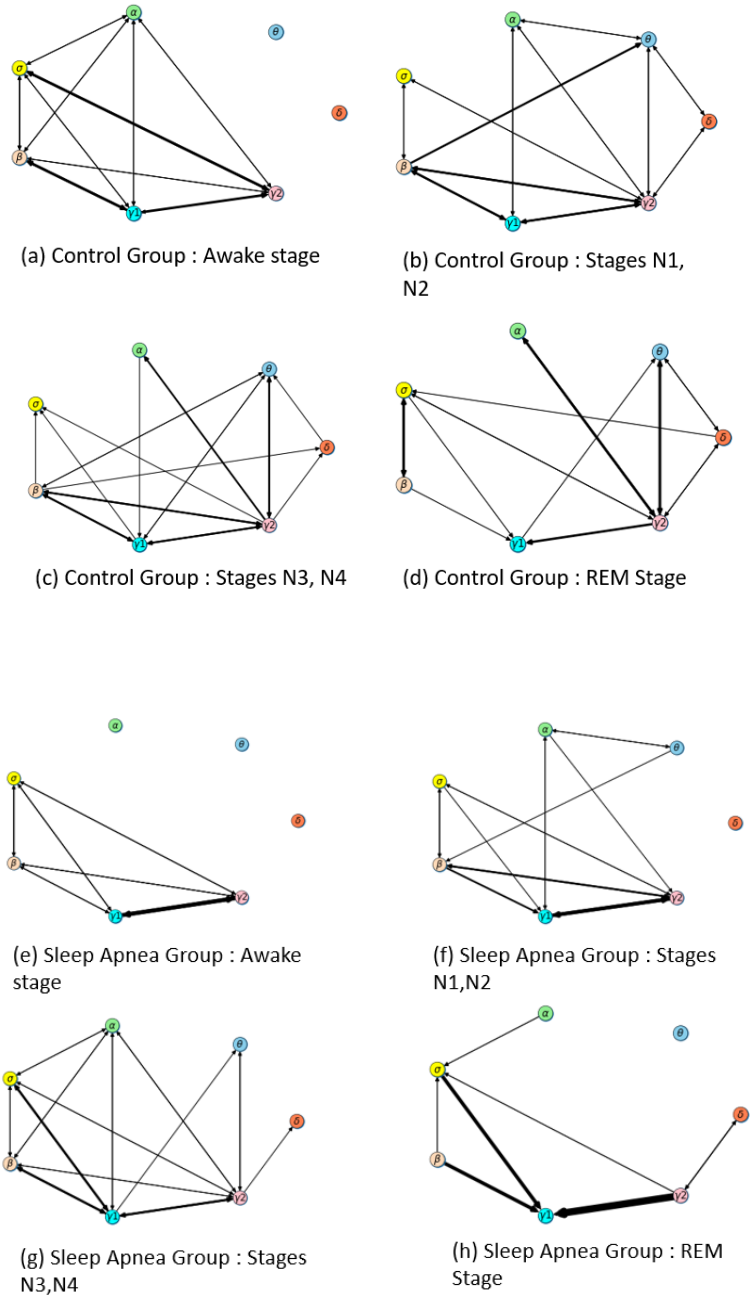

Figure 5.5: LSTMGC results for control group and sleep apnea group

5.6 Discussion

The brain is a significant organ that serves as the center of the nervous system and controls key organ systems. Depending on the physiologic state of the human body, the brain control mechanisms of different organ systems change. These control mechanisms are influenced by the sleep stage and the interactions among other brain regions during sleep. The brain regions communicate through various frequency bands, and a single frequency dominates each sleep stage. For instance, alpha waves are dominant in Awake and REM sleep stages; theta waves dominate in N1 and N2 sleep stages; delta waves are dominant in N3 and N4 sleep stages.

As a first step, we investigated the inter-brain network interactions in the brain C3 region in control and sleep apnea subjects during sleep. In order to identify the direction and strength of the intra-brain network interactions, we apply our two models, a) TDS to measure the strength of network links and b) LSTMGC to identify the direction of links to the EEG time series signals collected from the C3 brain region. Thus, we built a network with seven nodes where each node represents a frequency band among δ, θ, α, σ, β, $\gamma 1$ and $\gamma 2$. This work aims to identify the difference in intra-brain network interactions among control and sleep apnea subjects during different sleep stages.

We examine the strength and direction of all the 42 links, which are the combinations of all the possible edges between the intra-brain network nodes. The results indicate that the network structure of control and sleep apnea subjects in different sleep stages are described by different network structures. Furthermore, network structure changes significantly between control and sleep apnea subjects, with more network links found in control subjects.

Our analysis found that in all the sleep stages, the control subjects exhibited high connectivity compared to the sleep apnea subjects. In control subjects, the network connectivity is high during deep sleep (DS) and low during REM sleep. A similar pattern is seen among sleep apnea subjects during DS and REM sleep. In the Awake and light sleep (LS) sleep stages, the network structure

of control and sleep apnea subjects have similar links with identical link strengths. But the control subjects have more links compared to sleep apnea subjects. In REM sleep, some of the links present in the network structure of control subjects are absent in sleep apnea subjects.

When the direction of links is considered, both the control and sleep apnea subjects have mainly bidirectional links in the Awake sleep stage and more unidirectional links in the REM sleep stage. In the LS stage, some of the links are bidirectional in the network structure of control subjects but unidirectional in sleep apnea subjects.

5.7 Conclusion

Even though sleep is a resting state, sleep pathologies like sleep apnea impact the network connectivity between organ systems during sleep. We proposed a combination of TDS and LSTMGC method to identify the strength and direction of coupling between EEG frequency bands for control and sleep apnea subjects for different sleep stages. The results show a high coupling strength in control subjects in all sleep stages compared to sleep apnea subjects. Most links are bidirectional in the awake stage for control and sleep apnea subjects. However, in other sleep stages, more unidirectional links are identified in sleep apnea subjects, indicating a reduced coupling between EEG bands.

CHAPTER VI

PHASE III: ANALYSIS OF PHYSIOLOGICAL NETWORKS DURING SLEEP USING CONDITIONAL GRANGER CAUSALITY

This chapter discusses the influence of sao2 (oxygen saturation) and airflow (nasal airflow) signals on brain-heart interactions during sleep in sleep apnea and control subjects. Long-Short Term Memory based Conditional Granger Causality (LSTMCGC) method is used in this study to identify the indirect influence of a third organ signal on brain-heart interactions.

6.1 Introduction and Background work

For a healthy person, the oxygen saturation levels are between 95% and 100%. But, for a sleep apnea patient, the oxygen saturation levels drop as low as 70% [90] during an apnea event. The drop in oxygen saturation levels for a sleep apnea patient is shown in figure 6.1. The first graph shows the hypnogram where the y-axis specifies the sleep stages (0: Awake, 1: N1, 2: N2, 3:N3, 4:N4, and 5:REM). The second graph shows the oxygen saturation levels of the sleep apnea patient during the 8-hour long sleep. The lowest oxygen levels of the patient are seen during the REM sleep stage, where the levels drop to as low as 72%. The effects of such a drop in oxygen saturation levels on the interactions between organ systems during different sleep stages are largely unknown. As the airflow cessation [91] and reduction in oxygen saturation levels occur during sleep apnea episodes. In the current study, the indirect influences of sao2 and airflow signals on brain-heart interactions during different sleep stages are studied.

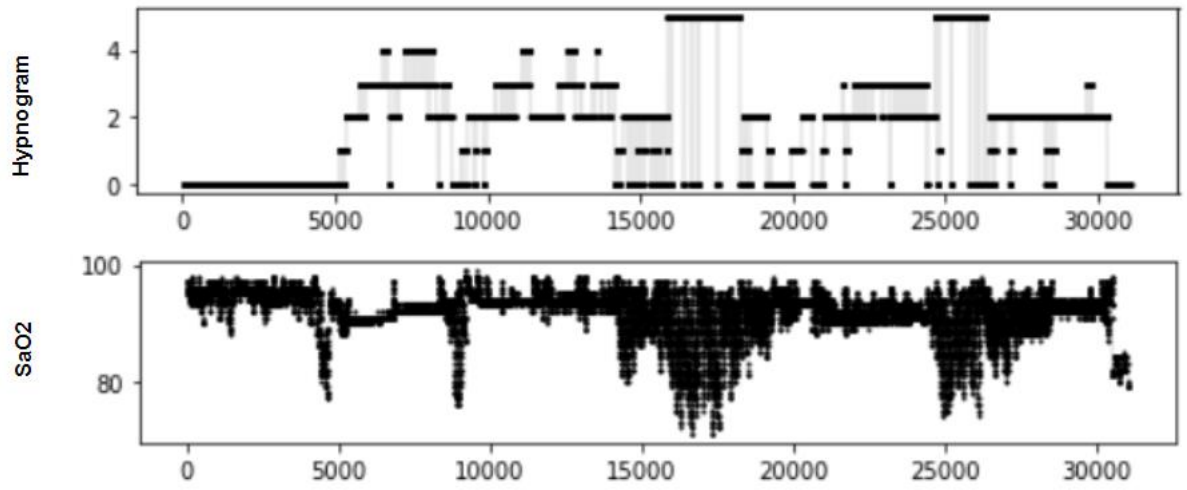

Figure 6.1: Hypnogram: X-Axis: Epoch value, Y-Axis: Sleep stage, SaO2: X-Axis: Epoch value, Y-Axis: Oxygen saturation level

Pairwise Granger causality methods are often used to identify causation between two time series signals [92]. However, the pairwise Granger causality methods do not clearly differentiate direct and indirect causal influences between two time series signals [93, 94]. The applications of conditional Granger causality in various fields are discussed below.

Granger causality model derived from autoregressive models has been actively used to determine the connectivity in the human brain with functional magnetic resonance imaging (fMRI) and to identify temporal and spatial dynamics of various cognitive processes. Zhou et al. [95] proposed a novel approach to quantify the connectivity in the brain using fMRI and the conditional granger causality model instead of a pairwise Granger causality model. The results demonstrate that conditional Granger causality could achieve better accuracy in identifying network connectivity compared to the more widely used pair-wise Granger causality model. Motor imagery has been

used widely to study the network reorganization of stroke-related patients. Wang et al.[96] proposed a framework to evaluate the cortical model networking patterns connectivity for stroke patients. In this study, conditional Granger causality is used to evaluate the connection between motor imagery and motor execution. The results demonstrate that a damaged hemisphere could cause abnormal motor activity during motor execution in stroke patients. Mainali et al. [97] proposed a conditional causal model detection for detecting interactions in human microbiome samples. The authors analyzed the duration and time series of the microbiome to decipher the network correlation and causation of microbial genera. The authors demonstrated Granger causality, and related techniques may be particularly helpful for understanding the governing nature of microbiome composition and structure. Gao et. al. [98] presented a framework that describes connectivity networks of motor execution and motor imagery using the conditional Granger causality model. The authors demonstrated that selected seed regions in the right-hand have performance higher than the left hand due to effective network connectivity resulting in the influence of brain asymmetry on connectivity networks. In addition, In-Out degrees consistently demonstrated the left lateralization for right-handed subjects. Conditional granger causality based on fMRI time series signals specifies how strongly certain portions of the brain contributes to the brain activity in a target region. Most efficient way to model nonlinear relationship between source and target brain signal is using conditional Granger causality. Chuang et. al. [99] proposed a framework based on deep stacking networks and convolution neural networks to understand the activities of the brain. Here, conditional Granger causality is used to assess the modelling fidelity based on convolution neural networks. The proposed technique successfully estimated time lags when synthetic datasets are applied. Thus, the proposed method based on conditional Granger causality is a promising model for complex brain networks. Ecological momentary assessment

(EMA) has been widely adopted in mobile health applications due to its valuable insights into many diseases. Conditional Granger causality based on EMA helps us understand the interpretation of a disease and its treatment decisions. Jamaludeen et al.[100] proposed a model based on conditional Granger causality and multivariate time series analysis to analyze EMA data of 270 users based on their registration data to determine conditional Granger causal relationships. The model discovered that some EMA items Granger cause others for more than 8% of the mobile health application users. Wada et. al. [101] implemented a conditional Granger causality test to analyze the connection between import, energy, export, economic growth, and population on environmental quality in Brazil. Conditional Granger causality is also applied to detect interaction networks in the human microbiome [102], and evaluate the effective connectivity of the resting-state networks [103].

To the best of our knowledge the conditional Granger causality approach has not applied to distinguish the influence of direct causal influences between two organ systems and indirect causal influences from a third organ system for sleep apnea subjects during sleep. As neural networks are capable of representing complex nonlinear and non-additive interactions between inputs and outputs, and as long short term memory (LSTM) networks have shown improved performance in forecasting multivariate time series given their past [88], in this study, we propose a LSTM based conditional Granger causality model. The LSTMCGC model implements conditional Granger causality to determine indirect causation of sao2 or airflow signals on causation between EEG frequency bands and heart rate signals collected through polysomnography. The aim of this analysis is to identify if:

1. the sao2 or airflow signals influence EEG frequency bands to cause changes to heart rate signals.

2. the sao2 or airflow signals influence heart rate signals to cause changes in EEG frequency bands.

The results indicate that during light sleep, the sao2 and airflow signals have a very low influence on brain-heart interactions in sleep apnea subjects but a strong influence in the control subjects, whereas in the REM sleep stage, the sao2 and airflow signals strongly influence brain-heart interactions for sleep apnea subjects, but very low influence for control subjects.

6.2 Model: LSTM based Conditional Granger Causality Estimation (LSTMCGC)

The influence of the airflow, sao2 signals on brain and heart interactions can be identified using LSTMCGC method where, LSTM is used in the principle of conditional Granger causality.

6.2.1 Conditional Granger Causality

In recent times, interest in the application of the Granger causality concept in physiology has increased significantly. The concept of Granger causality is utilized to identify the cause of a phenomena and also as a physiological marker [89, 104-108]. The concept of Granger causality and its application to identify interactions among brain networks during sleep is presented in 6.2. According to this approach, a direct causal relationship between time series X and Y as shown in figure 6.2 (where Y causes X, denoted by Y -> X) exists if the prediction error of X based on the past values of X and Y is statistically small compared to the prediction error of X when only past values of X is considered.

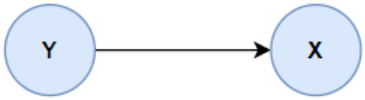

Figure 6.2: Direct Causality

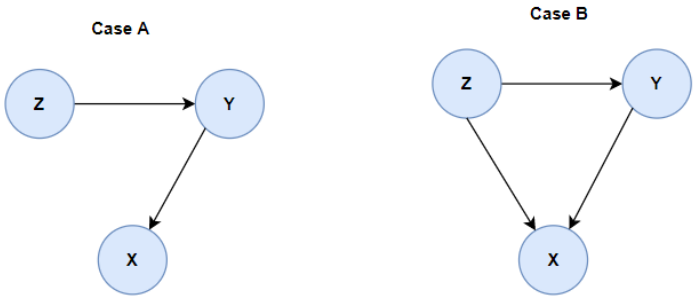

Figure 6.3: Case A: Full Indirect Causality, Case B: Partially Indirect Causality

But this causality analysis cannot identify some of the relationships between each pair of time series when three time series are considered. For instance, Z is the time-series signal causing Y, Y is the signal causing X, but Z is not causing X directly. In this case, if Granger causality is used to analyze direct relationships between two time series, the indirect causation between Z and X will be indistinguishable when Z is the signal causing Y and X (shown in figure 6.3). For both cases, A and B in figure 6.3, the causality analysis for two time series suggests the existence of relationships as presented in case B of figure 6.3.

A conditional Granger causality can be used to differentiate fully indirect causal relationships from partially indirect causal relationships in time series. According to conditional Granger causality, a fully indirect causal relationship between Z and X (where Z indirectly causes X through Y, denoted as Z -> X|Y) exists if the prediction error of X when the past values of X, Y, and Z is statistically smaller compared to the prediction error of X when only past values of Y and X are considered. For conditional Granger causal analysis, the equations depicted in equation 6 shown in section 5.4.1 can be extended by considering the third stochastic system Z_t and its respective coefficients as shown in equation (11).

$$Z_t = \sum_{j=1}^{p} c_1 Z_{t-j} + E_3 \tag{11}$$

where p is the maximum number of lagged observations, E_3 is residuals for Z series, c is the coefficient of the Z_t system. To find if series Z_t conditional Granger causes series X_t, an unrestricted prediction model of X_t combining with Y_t and Z_t is given as follows:

$$X_t = \sum_{j=1}^{p} a_3 X_{t-j} + \sum_{j=1}^{p} b_3 Y_{t-j} + \sum_{j=1}^{p} c_3 Z_{t-j} + E_1 \tag{12}$$

The conditional Granger causality from Z to X conditional on Y is given as shown in equation (13).

$$F_{Z \to X|Y} = ln \frac{\sigma^2 E_{XY}}{\sigma^2 E_{XYZ}} \tag{13}$$

where, $\sigma^2 E_{XY}$ means variance of the error obtained from the model when only past values of X, Y are considered and $\sigma^2 E_{XYZ}$ means variance of the error obtained from the model when past values of X, Y and Z are considered.

For conditional Granger causality analysis, two models are created as follows:

Model 1: Considering past values of *X* and *Y* to predict future values of *X* (Coefficients $c_3 = 0$ in equation (12)).

Model 2: Considering past values of *X*, *Y* and *Z* to predict future values of *X*.

Z causes *X* conditional on Y ($Z \rightarrow X|Y$) if the error E_1 for model 2 is significantly smaller than the error for model 1.

6.2.2 LSTMCGC

The architecture of the LSTMCGC model is shown in figure 6.4. Using the LSTMCGC model, the behavior of system X_t when past values of X_t and Y_t are considered and when past values of X_t, Y_t and Z_t are considered can be represented as shown in equation (9) in section 5.4.2 and equation (14) respectively.

$$X_t = f\left(\sum_{j=1}^{p} a_2 X_{t-j} + \sum_{j=1}^{p} b_2 Y_{t-j} + \sum_{j=1}^{p} c_2 Z_{t-j} + E_1\right) \quad (14)$$

where f is a nonlinear function, p is the maximum number of lagged observations, E_1 is the forecasting residues, *a, b* and *c* are the coefficients that relate to X_t, Y_t and Z_t systems respectively.

The conditional Granger causality for LSTMCGC model is measured as given in equation (15).

$$cgc = E_{xy} - E_{xyz} \quad (15)$$

Where, E_{xy} = forecasting error of model considering only X_t and Y_t as input.

E_{xyz} = forecasting error of model considering X_t, Y_t and Z_t as input.

If the c*gc* value is zero, then the system Z_t does not indirectly cause X_t. Positive c*gc* value refers to existence of effective indirect causation between systems Z_t to X_t.

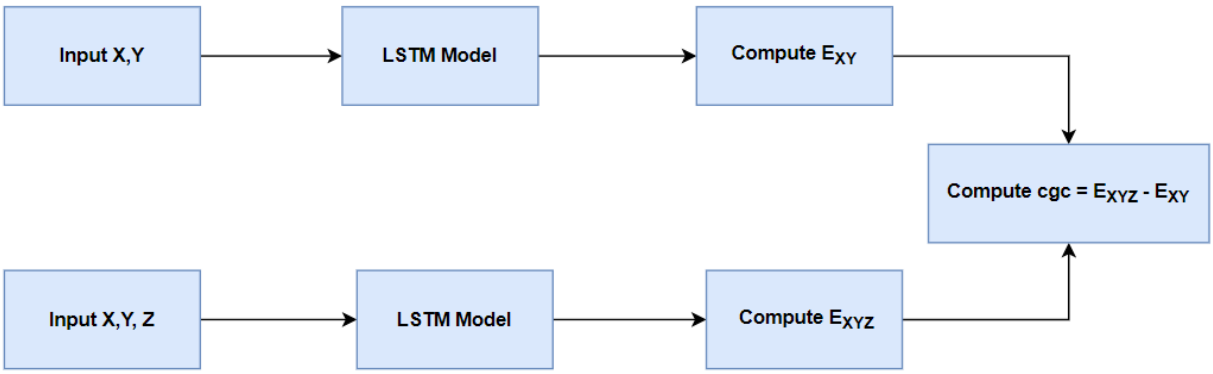

Figure 6.4: LSTMCGC Architecture

6.3 Results

For the current analysis, the EEG frequency bands, hr (heart rate), sao2 (oxygen saturation), airflow signals, and the hypnogram data of sleep apnea subjects (eight male, seven female) and control subjects (five male, five female) are considered. The EEG frequency bands are extracted from raw EEG signals, as shown in section 3.4. The sampling rate of hr, sao2, and airflow signals are resampled to 1Hz. After the preprocessing, all the time series signals have the same time resolution of 1 sec. The beginning and ending awake sleep stage data is removed for all the signals as the subject might be in a wakefulness state instead of an Awake sleep stage. The hypnogram data consists of Awake, N1, N2, N3, N4 and REM sleep stages. In the current study, the data of N1 and N2 sleep stages data is combined as Light Sleep (LS) and N3 and N4 sleep stages data is combined as Deep Sleep (DS).

For each subject, the following conditional Granger causal values are computed using the CCS algorithm:

a) ***sao2 --> hr | c***: Causal effect of *sao2* on *hr* signal conditional on signal *c*

b) ***sao2 --> c | hr:*** Causal effect of *sao2* on signal *c* conditional on *hr* signal

c) ***airflow --> hr | c:*** Causal effect of *airflow* signal on *hr* signal conditional on signal *c*

d) ***airflow --> c | hr:*** Causal effect of *airflow* on signal *c* conditional on *hr* signal

Signal *c* is a frequency band: $c \in \{\delta, \theta, \alpha, \beta, \sigma, \gamma1, \gamma2\}$

The graphs shown from figure 6.5 to 6.12 represent the results obtained for the current analysis. Each node in the graph represents a signal. The existence of an edge between nodes indicates the influence of sao2 or airflow on the interactions between the respective nodes. The direction of an edge between node1 $\rightarrow$ node2 indicates the conditional Granger causation of sao2 or airflow on node2 conditional on node1.

During AWAKE sleep stage, low conditional Granger causation from airflow signals to the different EEG frequency bands and hr signal interactions is observed (figures 6.5 and 6.6). But more conditional causal links are observed from sao2 signal to EEG frequency bands and hr signals. This indicates the influence of sao2 is higher than airflow on interactions between brain and heart interactions in AWAKE sleep stage in both control and sleep apnea subjects. A similar behavior of both sao2 and airflow signals is seen during deep sleep (figures 6.9 and 6.10).

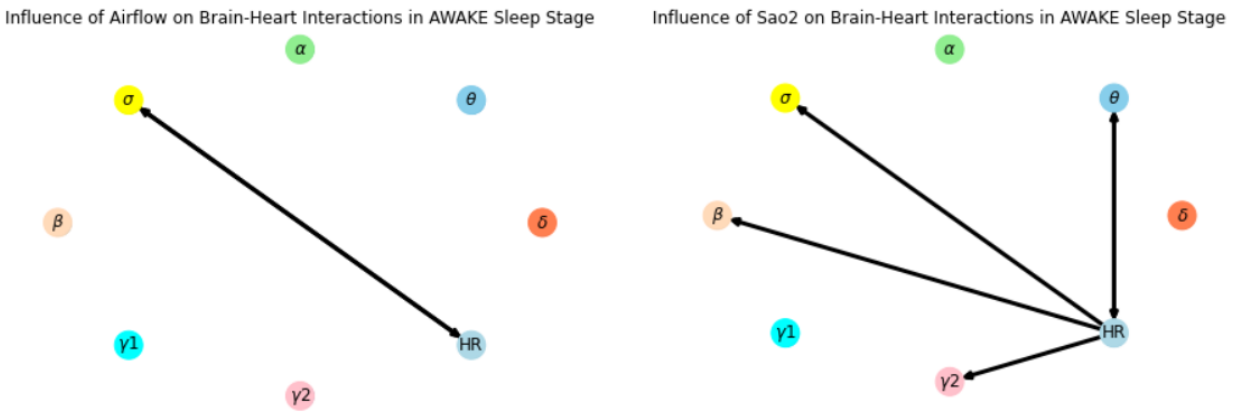

Figure 6.5: Network graphs for control subjects during AWAKE sleep stage

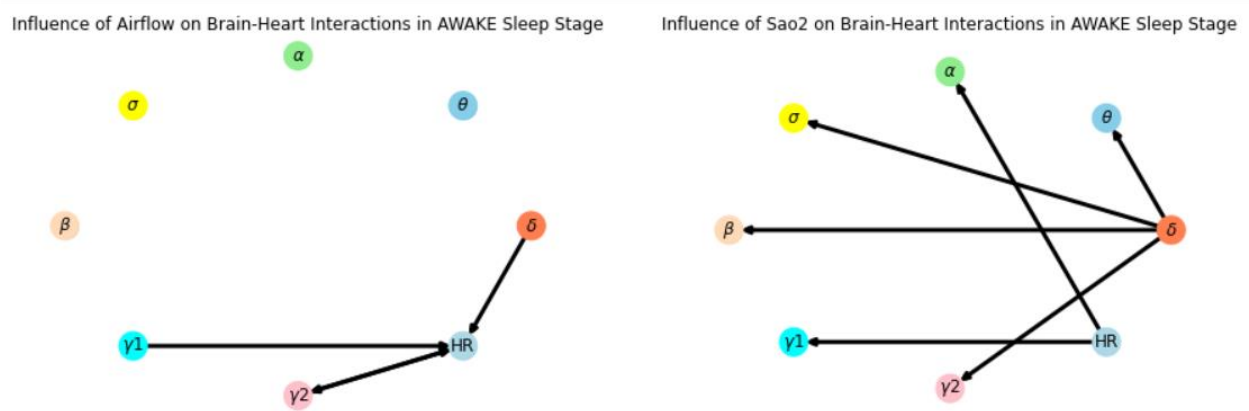

Figure 6.6: Network graphs for sleep apnea subjects during AWAKE sleep stage

During light sleep, more conditional causal links are seen between nodes when sao2 and airflow signal are considered for control subjects (Figure 6.7). But, for sleep apnea subjects, very few links are seen between nodes for both sao2 and airflow signals (figure 6.8). This indicates that during light sleep, both oxygen saturation levels and the airflow have an impact on the brain-heart interactions in control subjects. But such influence is minor in sleep apnea subjects.

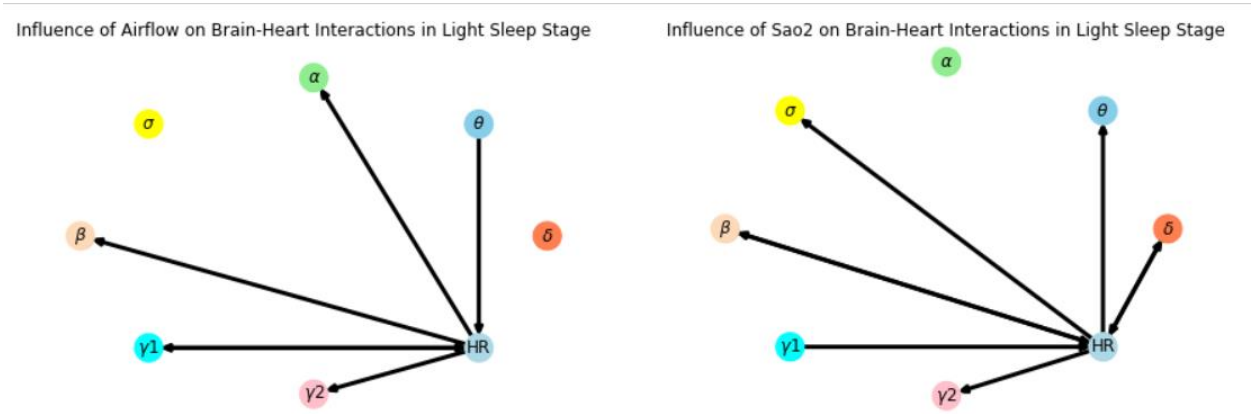

Figure 6.7: Network graphs for control subjects during Light Sleep

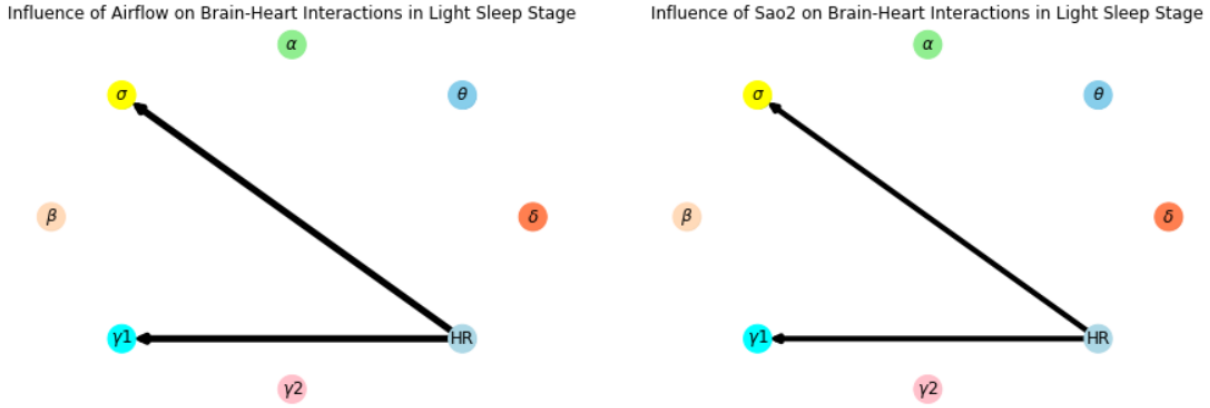

Figure 6.8: Network graphs for sleep apnea subjects during Light Sleep

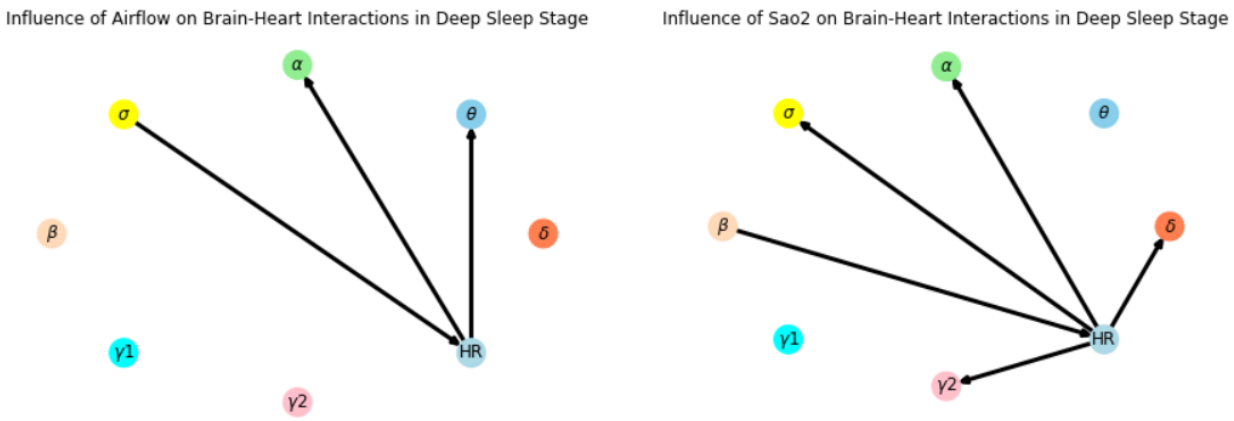

Figure 6.9: Network graphs for control subjects during Deep Sleep

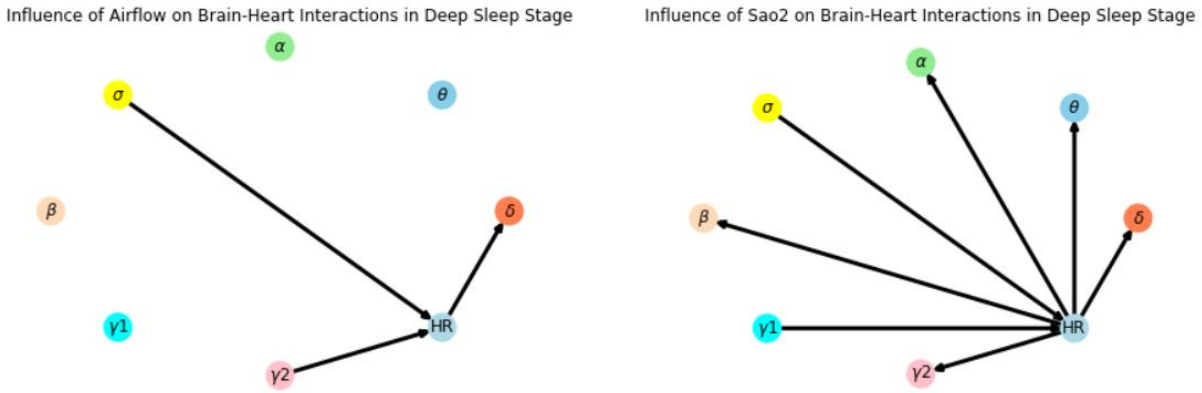

Figure 6.10: Network graphs for sleep apnea subjects during Deep Sleep stage

During the REM sleep stage, very few conditional causal links are observed between nodes for control subjects (figure 6.11), whereas for sleep apnea subjects, more conditional causal links are observed during the REM sleep stage (figure 6.12). This indicates that sao2 and airflow signals

have high influence during REM sleep stage in sleep apnea subjects when compared to the control subjects.

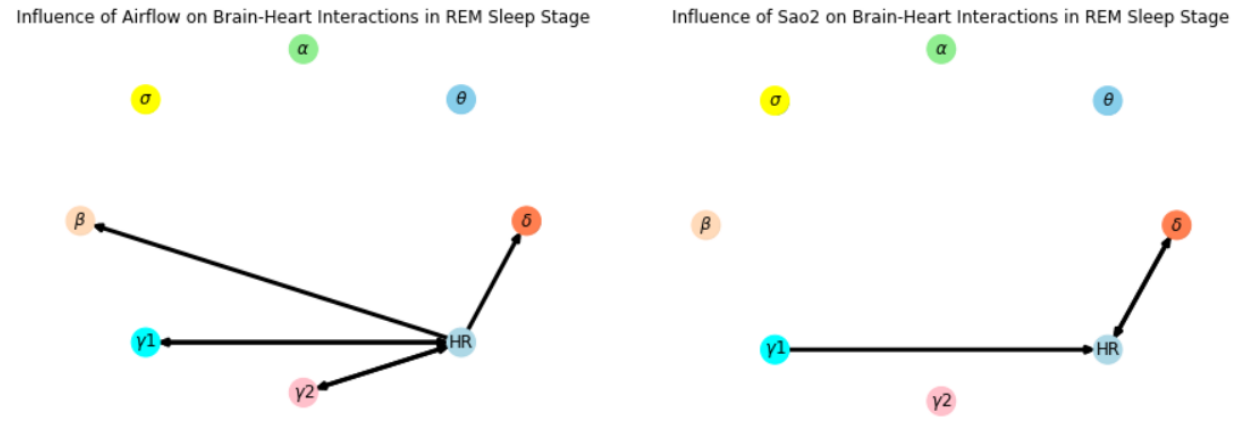

Figure 6.11: Network graphs for control subjects during REM sleep stage

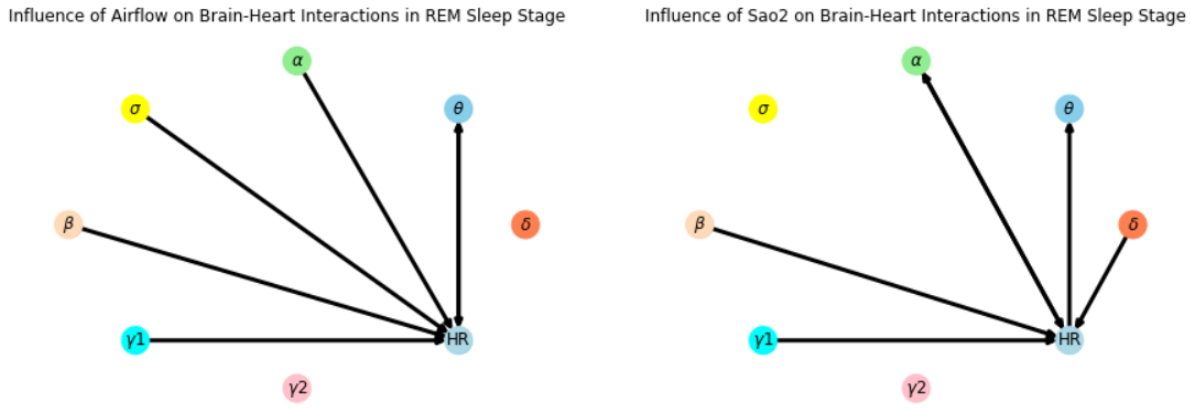

Figure 6.12: Network graphs for sleep apnea subjects during REM sleep stage

6.4 Conclusions

Conditional Granger causality analysis is used to explain the existence of an indirect influence caused by a third time-series signal on causal relationships between two time-series signals. In this study, the LSTMCGC method, which utilizes conditional Granger causality, is implemented to understand the influence of sao2 and airflow signals on brain-heart interactions during different sleep stages. The results indicate that during light sleep, sao2 and airflow signals have a very low influence on brain-heart interactions in sleep apnea subjects but a strong influence in the control subjects. In contrast, in the REM sleep stage, the sao2 and airflow signals strongly influence brain-heart interactions for sleep apnea subjects, but have very low influence for control subjects.

CHAPTER VII

PHASE IV: CHANGE IN CAUSATION BETWEEN SAO2 AND HR SIGNALS DURING SLEEP FOR SLEEP APNEA AND CONTROL SUBJECTS

This chapter discusses the changes in causation between two organ system signals over a night's sleep for a control subject and a sleep apnea subject. The changes in causation are identified using the Change in Causation during Sleep (CCS) method.

7.1 Introduction and Background work

Causal learning commonly determines the presence or absence of an influence from a driver time series to a target series. These causal influences determine whether the causation exists but does not explain when the causation occurs. But in public health, determining a causal influence and when the causal effect occurs can have profound consequences. For instance, smoking causes cancer, but the likelihood of individuals getting cancer increases over their lifetime. The concern here is not whether an individual is susceptible to cancer but when one might become vulnerable to it and if smoking increases the chances of it. In these cases, the concern is not on the occurrence of an event but its occurrence at or by a given time. Thus, the focus of this study is to address the question of when rather than whether an event occurs.

In most of the previous studies, researchers focused on identifying if an event occurs but did not consider the changes to the event over time [109]. Greville et. al. [110]. Performed a study to determine when rather than whether an event occurs. The authors conducted three experiments where the participants' actions can alter an outcome occurrence time. The overall results of this study indicate that participants are sensitive to event timing changes. Wasserman et. al. [111] conducted two experiments to study the role of temporal contiguity among college students responding to and rating contingency relations during operant conditioning. The students were given a task in which they gained points every time a light was illuminated, and the students could press a response key to influence the light. The students indicated a degree of sensitivity to changes in event timing. The overall results demonstrated the response and outcome contiguity as essential contributors to causal perception. According to the study by Greville et. al. [112, 113], postponing or advancing events in time was enough to obtain causal judgments from participants when the contingency was zero, thus suggesting that even when the statistical contingency is zero, the timing affects the causal perception.

Granger causality is commonly used to determine the causal influence of one time series on another. Granger causality is popularly applied in neurophysiological and functional imaging data to study the characteristics of neurons and brain-related activities. Wen et. al. [114] proposed a multivariate framework to estimate Granger causality based on matrix factorization. One of the advantages of this framework is that matrix estimation is needed only once for the multivariate dataset compared to autoregressive modeling, which requires estimation for each subset in the dataset. The Granger causality can be calculated by factorizing the submatrix of the overall matrix.

Granger causality is well known in fields like econometrics, where randomized tests are not exceptionally normal. Rather data about the powerful improvement of a framework is unequivocally demonstrated and used to characterize possibly causal relations. Also, the thought of causality as impact of mediations is transcendent in fields like clinical measurements or software engineering. Eichler et. al. [115] analyzed the impact of outer, potentially different and consecutive methods in an arrangement of multivariate time series using the Granger causal construction. The questions addressed by the authors include: a) under what interventions does Granger causality educate us about the effectiveness regarding interventions, and b) when does the observed times series permit to analyze this impact?

To the best of our knowledge, no study thus far has determined the changes in causal influences between two organ system signals over time for sleep apnea subjects during sleep.

The existence of causal influence indicates the possibility of intervention. In public health, it is not only important to determine if a causal effect exists but also when the causal influence occurs. During apnea events the body is denied of oxygen. Normal blood oxygenation is at 90%- 95%. An apnea event can drive that level into the 80's% or even 70's% [91]. These levels of oxygenation are damaging and dangerous. The impact of the reduced oxygen levels on other organ systems during sleep is largely unknown. In our current study, we studied the impact of oxygen saturation (sao2) on heart rate (hr) and vice-versa by using the CCS algorithm. The change in causation values from sao2 $\rightarrow$ hr and hr $\rightarrow$ sao2 are observed for an entire night sleep data for sleep apnea and control subjects. The results indicate that influence of oxygen saturation levels on heart rate for sleep apnea subjects is high during the REM sleep stage. But for control subjects, no such significant influence

during the REM sleep stage is seen. The causation of hr signals on sao2 signals is identified to be high during all sleep stages for control subjects.

7.2 Model: Change in Causation during Sleep (CCS)

The CCS algorithm determines the changes in causation between two organ system signals during an entire night's sleep for sleep apnea and control subjects. The steps for the CCS algorithm are shown in algorithm 7.1. Organ system signals like EEG, HR, SaO2, Airflow, etc., collected through polysomnography are provided as input to the model. Consider a target system *X* and driver system *Y*. The behavior of these systems can be represented using eq. (8) and (9) as described in section 5.4.2. In the CCS algorithm, similar to the LSTMGC method described in 5.4.2, Granger causality is used to determine the causality between a driver and target systems. But, in the CCS algorithm, the first sleep cycle (i.e., from the first AWAKE sleep stage to the end of the first REM sleep stage) is used as historical data for the LSTM neural network, as shown in figure 7.1.

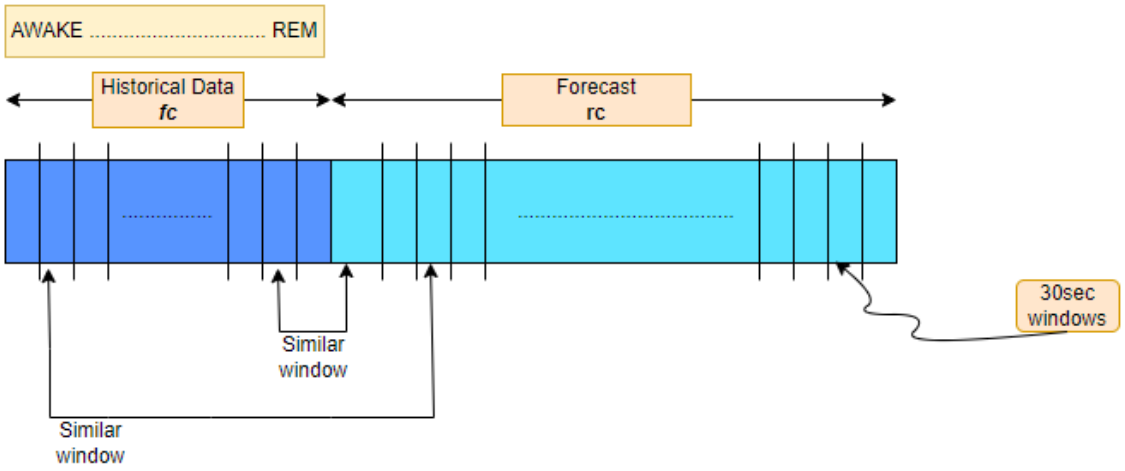

Figure 7.1: Data split for CCS model

The signals collected during the first sleep cycle are used as historical data to forecast the rest of the time-series signals, as shown in lines 15 through 18. The forecasted signal is split into *p* windows of duration 30sec. For each 30sec window, the Granger causality values are calculated as presented in equation 16 (line 19 to 26). The RMSEx (equation (16)) is the root mean squared error calculated when only past values of X are considered, and RMSExy (equation (17)) is the error computed when past values of both *X* and *Y* are considered.

$$Rmse_x = \sqrt{\frac{1}{len(\mathrm{p})}\sum_{t=p_t}^{t=p_t+30}(E_x)^2} \tag{16}$$

$$Rmse_{xy} = \sqrt{\frac{1}{len(\mathrm{p})}\sum_{t=p_t}^{t=p_t+30}(E_{xy})^2} \tag{17}$$

$$causality_{y\to x} = (\,2/1 + e^{\left(-\frac{RMSE_x}{RMSE_{xy}}+1\right)}) - 1 \tag{18}$$

where, p_t and p_{t+30} are the starting and ending times of the p^{th} window, E_x and E_{xy} are the forecasting residues.

However, the Granger causal values are available only for forecast data. The Granger causal values for the first sleep cycle are computed as shown in lines 27 to 33. The input signal is divided into two splits S_{fc} and S_{rc}, where S_{fc} consists of first sleep cycle data and S_{rc} consists of the rest of sleep cycles data (figure 7.1). The S_{fc} signal and S_{rc} signals are split *u* and *v* windows of 30sec duration

respectively. For each 30sec signal in window u of S_{fc}, its distance to all the v windows of S_{rc} are computed using the Euclidean distance measure. The similar window *(w_similar)* is determined as the window with minimum Euclidean distance (lines 1 to 14). The Granger causal value of the i^{th} window in S_{fc} is determined as the Granger causal value of its similar window $w\_similar[i]$ in S_{rc}.

The variables used in algorithm 7.1 are shown in table 7.1.

Table 7.1: Notations used in algorithm 7.1

Variable	**Purpose**
X, Y	Input signals
C_x	Granger causal values of signal Y -> X for every 30sec windows
S_{fc}, X_{fc}, Y_{fc}	First cycle (Awake to REM) data
S_{rc}, X_{rc}, Y_{rc}	Signal data from end of first cycle to the rest of the night
W_s	List of similar windows for all the 30sec windows of first cycle signal
dist	Distance matrix with distances of a window from first cycle signal to all the windows to the rest of the signal
$dist_{seg\_f}$	Euclidean distance
$dist_{min}$	Minimum Euclidean distance
$causality_{fc}$	Granger causality values for the signal Y -> X for the data of first cycle
$causality_{rc}$	Granger causality values for the signal Y -> X for the data after first cycle

$causality_p$	Granger causality for a 30sec window computed using equation 16
$Rmse_{xy}$	Error predicting X from past values of X,Y computed from equation 15
$Rmse_x$	Error predicting X from past values of X computed from equation 14
$S_{windows}$	Similar windows of the signals first cycle data

Algorithm 7.1: Change in Causation During Sleep

Input: Series *X*, Series *Y*

Output: C_x

---

1. **func** similar_windows(S_{fc}, S_{rc}):
2. split S_{fc} into *u* 30 sec windows
3. split S_{rc} into *v* 30 sec windows
4. W_s = [ ]
5. **for** each *seg_f* in *u* do:
6. *dist* = [ ]
7. **for** each *seg_r* in *v* do:
8. $dist_{seg\_f}$ = Euclidean distance (*seg_f*, *seg_r*)
9. dist.append($dist_{seg\_f}$)
10. **end for**
11. $dist_{min}$ = min of *dist*
12. *w_similar* = window of $dist_{min}$

13. W_s.append(*w_similar*)

14. **end for**

15. Split signal *X* into X_{fc} and X_{rc}

16. Split signal *Y* into Y_{fc} and Y_{rc}

17. Forecast *X*, given past values of *X*

18. Forecast *X*, given past values of *X*, *Y*

19. split X_{rc} into *p* 30sec windows

20. $causality_{rc}$ = [ ]

21. **for** each *p* do:

22. Compute $Rmse_x$

23. Compute $Rmse_{xy}$

24. Calculate $causality_p$

25. $causality_{rc}$.append($causality_p$)

26. **end for**

27. $S_{windows}$= *similar_windows*(X_{fc}, X_{rc})

28. split X_{fc} into *q* 30sec windows

29. $causality_{fc}$ = [ ]

30. **for** each *q* do:

31. $causality_q$ = *causality of* $S_{windows}[q]$

32. $causality_{fc}$.append($causality_p$)

33. **end for**

34. C_x = $causality_{fc}$ + $causality_{rc}$

7.3 Results

For the current analysis, sao2 signals, hr signals, and sleep stage hypnogram data of 7 male and 8 female sleep apnea and control subjects are considered from the available polysomnography data.

Data preprocessing is performed on the raw sao2 and hr signals where the beginning and ending awake sleep stage data is removed because the subject might be in a wakefulness state instead of an Awake sleep stage.

For each subject, the following causality changes are computed using the CCS algorithm:

a) sao2 --> hr: Causal effect of sao2 on hr signal

b) hr --> sao2: Causal effect of hr on sao2 signal.

7.3.1 Results for Sleep Apnea Subjects

The analysis is performed on all the available female and male sleep apnea subjects data. The results obtained for a single female and male sleep apnea subject is shown in figure 7.2 and figure 7.3, respectively. The first graph includes the causation values of sao2 $\rightarrow$> hr and hr $\rightarrow$ sao2 at each epoch. The second graph is a hypnogram which shows the sleep stage a subject is in during a given epoch. In the hypnogram, 0,1,2,3,4,5 indicates AWAKE, N1, N2, N3, N4 and REM sleep stages respectively. A common trend identified in all the sleep apnea subjects is that:

a) During the REM sleep stage, the causation from sao2 to hr signals is high for male and female subjects. Theoretically, sleep apnea episodes occur at high intensity during REM sleep stages.

The observed higher causal values from sao2 to hr signals indicate higher levels of influence of decreased oxygen levels on heart rate during sleep apnea episodes.

b) During light, deep, and Awake sleep stages, the causation from sao2 → hr is minimal for female subjects.

c) Except for the REM sleep stage, the hr → sao2 causal values are high compared to sao2 → hr causal values. But during the REM sleep stage, very high causal values are seen for sao2 → hr. This indicates that, for sleep apnea subjects, the influence of heart rate on oxygen saturation is high during awake, light and deep sleep stages.

d) For male and female sleep apnea subjects, the causality from sao2 to hr signals increases during REM sleep stage and decreases when the subject transitions from REM to other sleep stages.

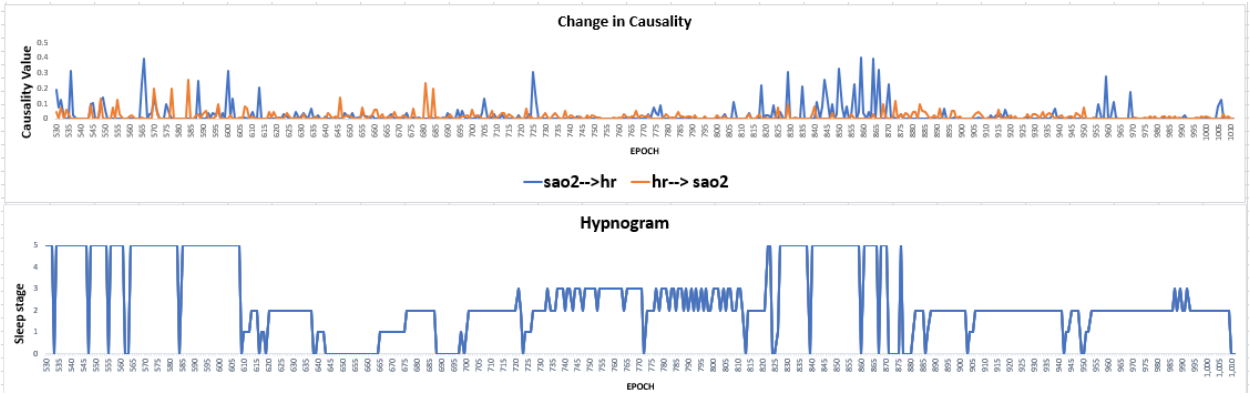

Figure 7.2: Change in causality for a female sleep apnea subject

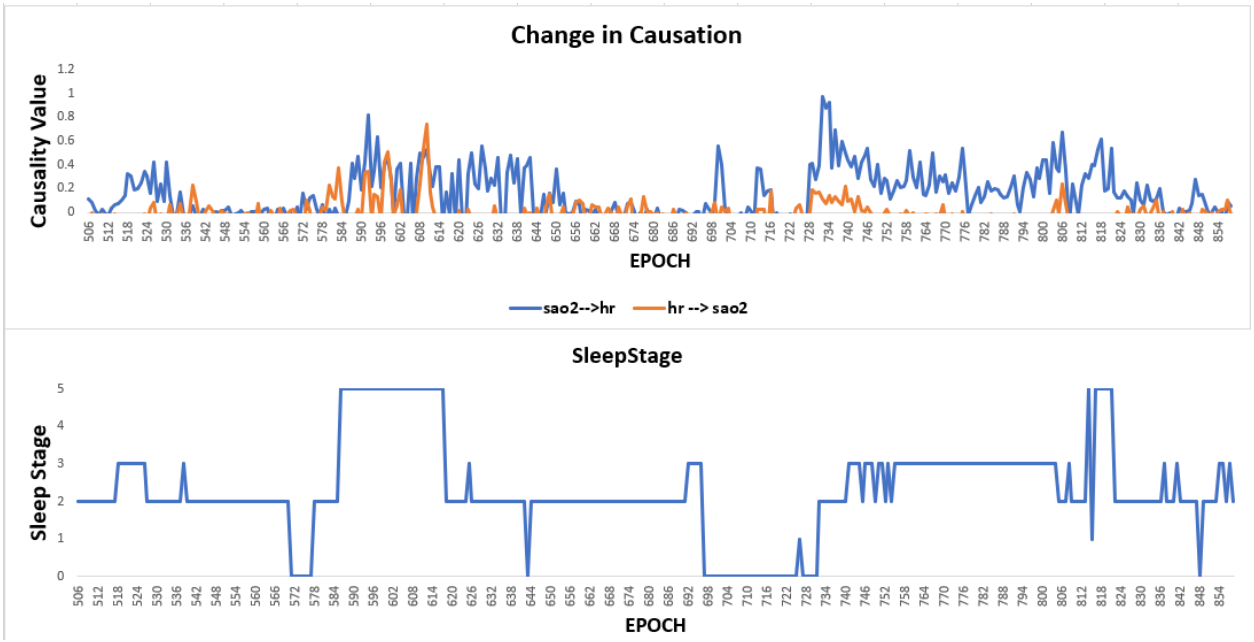

Figure 7.3: Change in causality for a male sleep apnea subject

7.3.2 Results for Control Subjects

The analysis is performed on all the available female and male control subject data. The obtained results for a single female and male sleep apnea subject is shown in figure 7.4 and figure 7.5, respectively. A common trend identified in all the control subjects is that:

a) In male control subjects, the hr → sao2 causal values are high compared to the sao2 → hr causal values in all sleep stages.

b) In male control subjects, no trend of higher sao2 → hr causal values during REM sleep is seen. In male control subjects, higher sao2 → hr causal values are seen during light sleep.

c) In female control subjects, overall sao2 → hr causation values are higher than the hr → sao2 causation values.

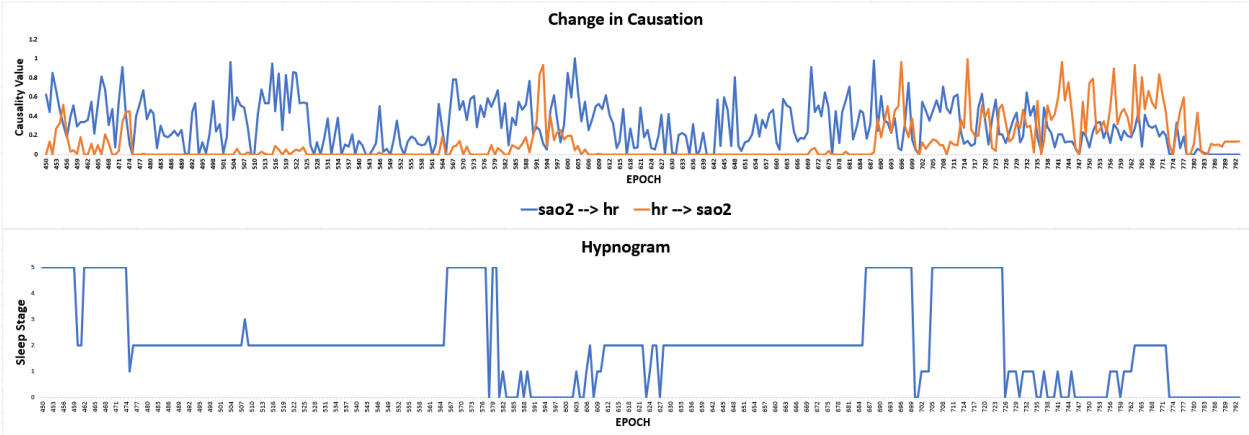

Figure 7.4: Change in causality for a female control subject

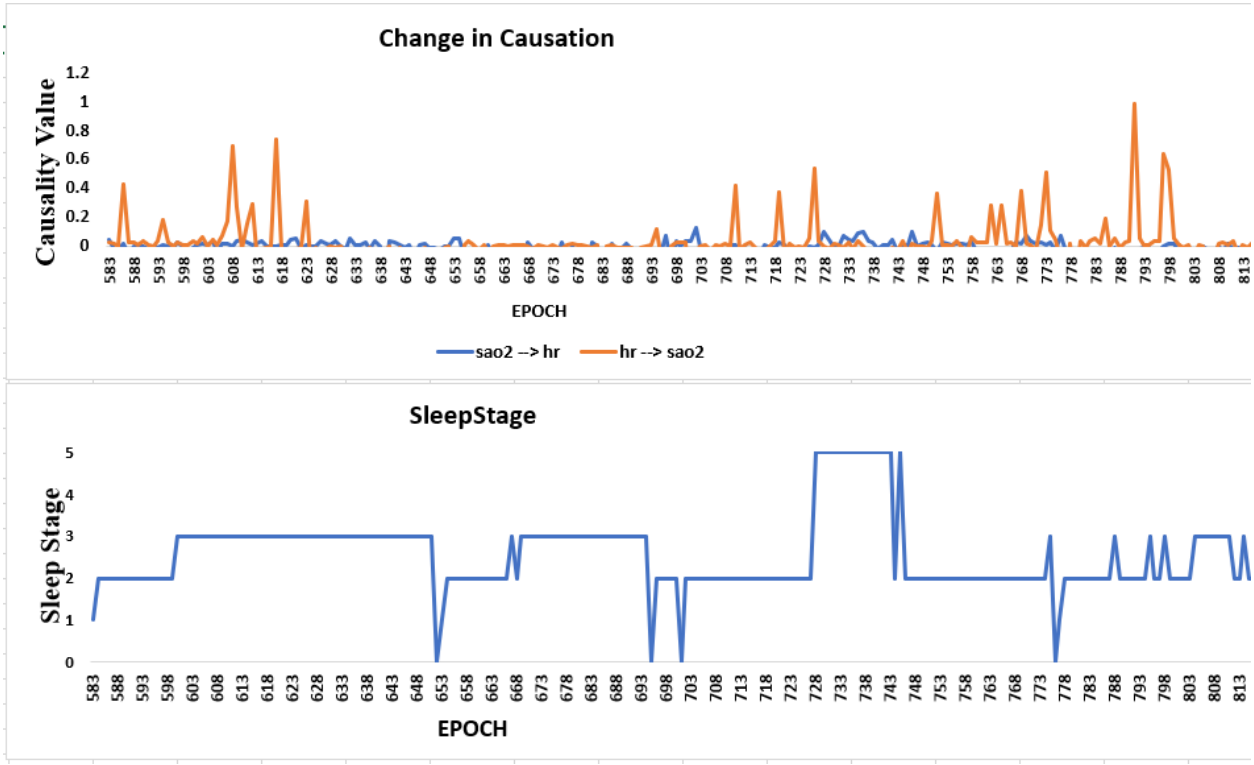

Figure 7.5: Change in causality for a male control subject

7.4 Conclusions

The existence of causal influence indicates the possibility of intervention. In public health, it is not only important to determine if a causal effect exists but also when the causal influence occurs. In the current study, we studied the impact of oxygen saturation on heart rate and vice-versa by using the CCS algorithm. The change in causation values from sao2 → hr and hr → sao2 are observed in the entire night's sleep data for sleep apnea and control subjects. The results indicate that influence of oxygen saturation levels on heart rate for sleep apnea subjects is high during the REM sleep stage. But for control subjects, no such significant influence during the REM sleep stage is seen.

The causation of hr signals on sao2 signals is identified to be high during all sleep stages for control subjects.

REFERENCES

[1] Cárdenas, J., Orjuela-Cañón, A.D., Cerquera, A., and Ravelo, A.: 'Characterization of physiological networks in sleep apnea patients using artificial neural networks for Granger causality computation', in Proceedings of SPIE, 13th International Conference on Medical Information Processing and Analysis, pp. 406-412, 2017

[2] Walker, M.P., 'The role of sleep in cognition and emotion', Annals of the New York Academy of Sciences, 1156, (1), pp. 168-197, 2009

[3] Walker MP, Stickgold R., Sleep, memory, and plasticity. Annu. Rev. Psychol.., Vol 57; pp 139-166, doi: 10.1146/annurev.psych.56.091103.070307. PMID: 16318592, 2006

[4] Backhaus, J., Hoeckesfeld, R., Born, J., Hohagen, F., and Junghanns, K.: 'Immediate as well as delayed post learning sleep but not wakefulness enhances declarative memory consolidation in children', Neurobiology of learning and memory, 2008, 89, (1), pp. 76-80

[5] Kopasz, M., Loessl, B., Hornyak, M., Riemann, D., Nissen, C., Piosczyk, H., and Voderholzer, U.: 'Sleep and memory in healthy children and adolescents–a critical review', Sleep medicine reviews, 2010, 14, (3), pp. 167-177

[6] Wilhelm, I., Diekelmann, S., and Born, J.: 'Sleep in children improves memory performance on declarative but not procedural tasks', Learning & memory, pp. 373-377, 2008

[7] Morselli, L., Leproult, R., Balbo, M., and Spiegel, K., 'Role of sleep duration in the regulation of glucose metabolism and appetite', Best practice & research Clinical endocrinology & metabolism, 24(5), pp. 687-702, 2010

[8] St-Onge, Marie-Pierre., 'The role of sleep duration in the regulation of energy balance: effects on energy intakes and expenditure', Journal of Clinical Sleep Medicine, 9(1) pp. 73-80, 2013

[9] Cappuccio, F., Miller, M.A., and Lockley, S.W., 'Sleep, health, and society: From aetiology to public health', Oxford University Press, USA, 2010

[10] Al Khatib, H., Harding, S., Darzi, J., and Pot, G., 'The effects of partial sleep deprivation on energy balance: a systematic review and meta-analysis', European journal of clinical nutrition, 71(5), pp. 614-624, 2017

[11] Obstructive Sleep Disordered Breathing, https://www.ncbi.nlm.nih.gov/books/NBK19956/, (date of last acess 05/01/2022)

[12] Loomis, A.L., Harvey, E.N., and Hobart, G.A., 'Cerebral states during sleep, as studied by human brain potentials', Journal of Experimental Psychology, 21(2), pp. 127-144, 1937

[13] Dement, W., and Kleitman, N., 'Cyclic variations in EEG during sleep and their relation to eye movements, body motility, and dreaming', Electroencephalogr Clin Neurophysiol, 9(4), pp. 673-690, 1957

[14] Carskadon, M.A., and Dement, W.C., 'Normal human sleep: an overview', Principles and practice of sleep medicine, 4(1), pp. 13-23, 2005

[15] Gais, S., Mölle, M., Helms, K., and Born, J., 'Learning-dependent increases in sleep spindle density', J Neurosci, 22(15), pp. 6830-6834, 2002

[16] Kryger, M.H., Roth, T., and Dement, W.C., 'Principles and Practice of Sleep Medicine E-Book', Elsevier Health Sciences, 2010

[17] The importance of sleep, https://edocs.southglos.gov.uk/sleeptoolkit-earlyyears/pages/introduction-the-importance-of-sleep/, (date of last 06/01/2022)

[18] Buysse, Daniel J., 'Sleep Health: Can We Define It? Does It Matter?', Sleep, 37(1), pp. 9-17, 2014

[19] Matricciani, L., Bin, Y.S., Lallukka, T., Kronholm, E., Dumuid, D., Paquet, C., and Olds, T., 'Past, present, and future: trends in sleep duration and implications for public health', Sleep health, 3(5), pp. 317-323, 2017

[20] Matricciani, L., Paquet, C., Galland, B., Short, M., and Olds, T., 'Children's sleep and health: a meta-review', Sleep medicine reviews, 46, pp. 136-150, 2019

[21] Matricciani, L., Bin, Y.S., Lallukka, T., Kronholm, E., Wake, M., Paquet, C., Dumuid, D., and Olds, T., 'Rethinking the sleep-health link', Sleep health, 4(4), pp. 339-348, 2018

[22] Walker, M.: 'Why we sleep: Unlocking the power of sleep and dreams', Simon and Schuster, 2017

[23] American Sleep Association, https://www.sleepassociation.org/about-sleep/what-is-sleep/, (date of last access 06/01/2022)

[24] Hirshkowitz, M., Whiton, K., Albert, S.M., Alessi, C., Bruni, O., DonCarlos, L., Hazen, N., Herman, J., Katz, E.S., Kheirandish-Gozal, L., Neubauer, D.N., O'Donnell, A.E., Ohayon, M., Peever, J., Rawding, R., Sachdeva, R.C., Setters, B., Vitiello, M.V., Ware, J.C., and Adams Hillard, P.J., 'National Sleep Foundation's sleep time duration recommendations: methodology and results summary', Sleep Health, 1(1), pp. 40-43, 2015

[25] Hoevenaar-Blom, M.P., Spijkerman, A.M., Kromhout, D., van den Berg, J.F., and Verschuren, W.M., 'Sleep duration and sleep quality in relation to 12-year cardiovascular disease incidence: the MORGEN study', Sleep, 34(11), pp. 1487-1492, 2011

[26] Dean, D.A., 2nd, Goldberger, A.L., Mueller, R., Kim, M., Rueschman, M., Mobley, D., Sahoo, S.S., Jayapandian, C.P., Cui, L., Morrical, M.G., Surovec, S., Zhang, G.Q., and

Redline, S., ‘Scaling Up Scientific Discovery in Sleep Medicine: The National Sleep Research Resource’, Sleep, 39(5), pp. 1151-1164, 2016

[27] Matsumoto, T., and Chin, K.: ‘Prevalence of sleep disturbances: sleep disordered breathing, short sleep duration, and non-restorative sleep’, Respiratory investigation, 57(3), pp. 227-237, 2019

[28] Sleep in America Poll, https://www.sleepfoundation.org/wp-content/uploads/2018/10/2009-POLL-HIGHLIGHTS.pdf, (date of last access 05/10/2022)

[29] Steptoe, A., Peacey, V., and Wardle, J., ‘Sleep duration and health in young adults’, Archives of internal medicine, 166(16), pp. 1689-1692, 2006

[30] Stranges, S., Dorn, J.M., Shipley, M.J., Kandala, N.-B., Trevisan, M., Miller, M.A., Donahue, R.P., Hovey, K.M., Ferrie, J.E., and Marmot, M.G., ‘Correlates of short and long sleep duration: a cross-cultural comparison between the United Kingdom and the United States: the Whitehall II Study and the Western New York Health Study’, American journal of epidemiology, 168(12), pp. 1353-1364, 2008

[31] Beihl, D.A., Liese, A.D., and Haffner, S.M., ‘Sleep duration as a risk factor for incident type 2 diabetes in a multiethnic cohort’, Annals of epidemiology, 19(5), pp. 351-357, 2009

[32] Gottlieb, D.J., Punjabi, N.M., Newman, A.B., Resnick, H.E., Redline, S., Baldwin, C.M., and Nieto, F.J., ‘Association of sleep time with diabetes mellitus and impaired glucose tolerance’, Archives of internal medicine, 165(8), pp. 863-867, 2005

[33] Knutson, K.L., Ryden, A.M., Mander, B.A., and Van Cauter, E.: ‘Role of sleep duration and quality in the risk and severity of type 2 diabetes mellitus’, Archives of internal medicine, 166(16), pp. 1768-1774, 2006

[34] Hall, M.H., Muldoon, M.F., Jennings, J.R., Buysse, D.J., Flory, J.D., and Manuck, S.B., ‘Self-reported sleep duration is associated with the metabolic syndrome in midlife adults’, Sleep, 31(5), pp. 635-643, 2008

[35] Cappuccio, F.P., Taggart, F.M., Kandala, N.-B., Currie, A., Peile, E., Stranges, S., and Miller, M.A. 'Meta-analysis of short sleep duration and obesity in children and adults', Sleep, 31(5), pp. 619-626, 2008

[36] Cohen, S., Doyle, W.J., Alper, C.M., Janicki-Deverts, D., and Turner, R.B., 'Sleep habits and susceptibility to the common cold', Archives of internal medicine, 169(1), pp. 62-67, 2009

[37] Patel, S.R., Zhu, X., Storfer-Isser, A., Mehra, R., Jenny, N.S., Tracy, R., and Redline, S., 'Sleep duration and biomarkers of inflammation', Sleep, 32(2), pp. 200-204, 2009

[38] Irwin, M.R., 'Why sleep is important for health: a psychoneuroimmunology perspective', Annual review of psychology, 66, pp. 143, 2015

[39] Ayas, N.T., White, D.P., Manson, J.E., Stampfer, M.J., Speizer, F.E., Malhotra, A., and Hu, F.B., 'A prospective study of sleep duration and coronary heart disease in women', Archives of internal medicine, 163(2), pp. 205-209, 2003

[40] Gottlieb, D.J., Redline, S., Nieto, F.J., Baldwin, C.M., Newman, A.B., Resnick, H.E., and Punjabi, N.M., 'Association of usual sleep duration with hypertension: the Sleep Heart Health Study', Sleep, 29(8), pp. 1009-1014, 2006

[41] Gangwisch, J.E., Heymsfield, S.B., Boden-Albala, B., Buijs, R.M., Kreier, F., Pickering, T.G., Rundle, A.G., Zammit, G.K., and Malaspina, D., 'Short sleep duration as a risk factor for hypertension: analyses of the first National Health and Nutrition Examination Survey', hypertension, 47(5), pp. 833-839, 2006

[42] Asplund, R., 'Sleep disorders in the elderly', Drugs & Aging, 14(2), pp. 91-103, 1999

[43] Sleep Apnea Information for Clinicians, https://www.sleepapnea.org/learn/sleep-apnea-information-clinicians/, (date of last access 06/01/2022)

[44] White, D.P., 'Sleep apnea', Proceedings of the American Thoracic Society, 3(1), pp. 124-128, 2006

[45] Strollo Jr, P.J., and Rogers, R.M., 'Obstructive sleep apnea', New England Journal of Medicine, 334(2), pp. 99-104, 1996

[46] Economic burden of undiagnosed sleep apnea in U.S. is nearly $150B per year, https://aasm.org/economic-burden-of-undiagnosed-sleep-apnea-in-u-s-is-nearly-150b-per-year/, (date of last access 06/01/2022)

[47] Rundo, J.V., and Downey, R., 'Chapter 25 - Polysomnography', in Levin, K.H., and Chauvel, P. (Eds.): 'Handbook of Clinical Neurology', Elsevier, 2019, pp. 381-392

[48] Measuring Sleep, https://slideplayer.com/slide/8533676/, (date of last access 06/01/2022)

[49] Kudlow, P.A., Cha, D.S., Lam, R.W., and McIntyre, R.S., 'Sleep architecture variation: a mediator of metabolic disturbance in individuals with major depressive disorder', Sleep Med, 14(10), pp. 943-949, 2013

[50] Altevogt, B.M., and Colten, H.R., 'Sleep disorders and sleep deprivation: an unmet public health problem', 2006

[51] Yaremchuk, K.L., and Wardrop, P.A., 'Sleep medicine', Plural Publishing, 2010

[52] Bartsch, R.P., Liu, K.K.L., Bashan, A., and Ivanov, P.C., 'Network Physiology: How Organ Systems Dynamically Interact', PloS One, 10(11), pp. e0142143,2015

[53] Faes, L., Marinazzo, D., Jurysta, F., and Nollo, G., 'Granger causality analysis of sleep brain-heart interactions', 8th Conference of the European Study Group on Cardiovascular Oscillations (ESGCO), IEEE, pp. 5-6, 2014

[54] Zhang, G.-Q., Cui, L., Mueller, R., Tao, S., Kim, M., Rueschman, M., Mariani, S., Mobley, D., and Redline, S., 'The National Sleep Research Resource: towards a sleep data commons', Journal of the American Medical Informatics Association, 25(10), pp. 1351-1358, 2018

[55] Quan, S.F., Howard, B.V., Iber, C., Kiley, J.P., Nieto, F.J., O'Connor, G.T., Rapoport, D.M., Redline, S., Robbins, J., and Samet, J.M., 'The sleep heart health study: design, rationale, and methods', Sleep, 20(12), pp. 1077-1085, 1997

[56] Redline, S., Sanders, M., Lind, B., Quan, S., Iber, C., Gottlieb, D., Bonekat, W., Rapoport, D., Smith, P., and Kiley, J., 'Sleep Heart Health Research Group Methods for obtaining and analyzing unattended polysomnography data for a multicenter study', Sleep, 21(7), pp. 759-767, 1998

[57] Sleep Heart Health Study, https://sleepdata.org/datasets/shhs/pages/full-description.md, (date of last access 06/01/2022)

[58] Understanding Sleep Cycles and Stages of Sleep, https://www.whoop.com/thelocker/stages-of-sleep-cycles/, (date of last access 06/01/2022)

[59] The Science of Sleep: Stages and Cycles, https://www.helpguide.org/harvard/biology-of-sleep-circadian-rhythms-sleep-stages.html, (date of last access 05/01/2022)

[60] Christensen, J.A.E., Carrillo, O., Leary, E.B., Peppard, P.E., Young, T., Sorensen, H.B.D., Jennum, P., and Mignot, E., 'Sleep-stage transitions during polysomnographic recordings as diagnostic features of type 1 narcolepsy', Sleep medicine, 16(12), pp. 1558-1566, 2015

[61] Laffan, A., Caffo, B., Swihart, B.J., and Punjabi, N.M., 'Utility of sleep stage transitions in assessing sleep continuity', Sleep, 33(12), pp. 1681-1686, 2010

[62] Schlemmer, A., Parlitz, U., Luther, S., Wessel, N., and Penzel, T., 'Changes of sleep-stage transitions due to ageing and sleep disorder', Philosophical Transactions of the Royal Society A: Mathematical, Physical and Engineering Sciences, 373(2034), pp. 20140093, 2015

[63] Kim, J.-C., and Chung, K.: 'Mining based time-series sleeping pattern analysis for life big-data', Wireless Personal Communications, 105(2), pp. 475-489, 2019

[64] Masseglia, F., Teisseire, M., and Poncelet, P., ‘Sequential pattern mining’: ‘Encyclopedia of data warehousing and mining’ ,IGI Global, pp. 1028-1032, 2005

[65] Agrawal, R., and Srikant, R.: ‘Fast algorithms for mining association rules’, Proc. 20th int. conf. very large data bases, VLDB, 1215, pp. 487-499. 1994

[66] Gopalan, N., and Sivaselvan, B., ‘Data Mining: Techniques and Trends’, PHI Learning Private Limited, 2009

[67] Hegland, M., ‘The apriori algorithm–a tutorial’, Mathematics and computation in imaging science and information processing, pp. 209-262, 2007

[68] Yabing, J., ‘Research of an improved apriori algorithm in data mining association rules’, International Journal of Computer and Communication Engineering, 2(1), pp. 25, 2013

[69] de Zambotti, M., Trinder, J., Silvani, A., Colrain, I.M., and Baker, F.C., ‘Dynamic coupling between the central and autonomic nervous systems during sleep: a review’, Neuroscience & Biobehavioral Reviews, 90, pp. 84-103, 2018

[70] Ivanov, P.C., Liu, K.K., Lin, A., and Bartsch, R.P., ‘Network physiology: from neural plasticity to organ network interactions’: ‘Emergent complexity from nonlinearity, in physics, engineering and the life sciences’, Springer, pp. 145-165, 2017

[71] Amblard, P.-O., and Michel, O.J., ‘On directed information theory and Granger causality graphs’, Journal of computational neuroscience, 30(1), pp. 7-16, 2011

[72] Vicente, R., Wibral, M., Lindner, M., and Pipa, G., ‘Transfer entropy—a model-free measure of effective connectivity for the neurosciences’, Journal of computational neuroscience, 30(1), pp. 45-67, 2011

[73] Runge, J., Heitzig, J., Petoukhov, V., and Kurths, J., ‘Escaping the curse of dimensionality in estimating multivariate transfer entropy’, Physical review letters, 108(25), pp. 258701, 2012

[74] Granger, C.W., ‘Investigating causal relations by econometric models and cross-spectral methods’, Econometrica: journal of the Econometric Society, pp. 424-438, 1969

[75] Lütkepohl, H.: ‘New introduction to multiple time series analysis’, Springer Science & Business Media, 2005

[76] Sameshima, K., and Baccala, L.A., ‘Methods in brain connectivity inference through multivariate time series analysis’, CRC press, 2014

[77] Lozano, A.C., Abe, N., Liu, Y., and Rosset, S., ‘Grouped graphical Granger modeling methods for temporal causal modeling’, Proceedings of the 15th ACM SIGKDD international conference on Knowledge discovery and data mining, pp. 577-586, 2009

[78] Nicholson, W.B., Wilms, I., Bien, J., and Matteson, D.S., ‘High Dimensional Forecasting via Interpretable Vector Autoregression’, J. Mach. Learn. Res., 21(166), pp.1-52, 2020

[79] Shojaie, A., and Michailidis, G., ‘Discovering graphical Granger causality using the truncating lasso penalty’, Bioinformatics, 26(18), pp. i517-i523, 2010

[80] Lusch, B., Maia, P.D., and Kutz, J.N., ‘Inferring connectivity in networked dynamical systems: Challenges using Granger causality’, Physical Review E, 94(3), pp. 032220, 2016

[81] Tong, H., ‘Nonlinear time series analysis’: ‘International Encyclopedia of Statistical Science’ ,Springer, pp. 955-958, 2011

[82] Terasvirta, T., Tjostheim, D., and Granger, C.W., ‘Modelling nonlinear economic time series’, OUP Catalogue, 2010

[83] Billings, S.A., ‘Nonlinear system identification: NARMAX methods in the time, frequency, and spatio-temporal domains’, John Wiley & Sons, 2013

[84] Kişi, Ö., ‘River flow modeling using artificial neural networks’, Journal of Hydrologic Engineering, 9(1), pp. 60-63, 2004

[85] Raissi, M., Perdikaris, P., and Karniadakis, G.E., ‘Multistep neural networks for data-driven discovery of nonlinear dynamical systems’, arXiv preprint arXiv:1801.01236, 2018

[86] Graves, A., ‘Supervised sequence labelling’: ‘Supervised sequence labelling with recurrent neural networks’, Springer, pp. 5-13, 2012

[87] Tank, A., Covert, I., Foti, N., Shojaie, A., and Fox, E., 'Neural granger causality', arXiv preprint arXiv:1802.05842, 2018

[88] Tank, A., Covert, I., Foti, N., Shojaie, A., and Fox, E., 'Neural granger causality for nonlinear time series', stat, 1050, pp. 16, 2018

[89] Orjuela-Cañón, A.D., Cerquera, A., Freund, J.A., Juliá-Serdá, G., and Ravelo-García, A.G., 'Sleep apnea: Tracking effects of a first session of CPAP therapy by means of Granger causality', Computer Methods and Programs in Biomedicine, 187, pp. 105235, 2020

[90] Sleep Apnea, https://www.chasedentalsleepcare.com/contents/sleep-sickness/sleep-apnea-overview, (date of last access 05/01/2022)

[91] Obstructive Sleep Disordered Breathing, https://www.ncbi.nlm.nih.gov/books/NBK441909/, (date of last access 05/012022)

[92] Awe, O.O., 'On pairwise granger causality modelling and econometric analysis of selected economic indicators', Interstatt journals. net/YEAR/2012/articles/1208002. pdf, 2012

[93] Marica, V.G., and Horobet, A., 'Conditional Granger Causality and Genetic Algorithms in VAR Model Selection', Symmetry, 11(8), pp. 1004, 2019

[94] Chen, Y., Bressler, S.L., and Ding, M., 'Frequency decomposition of conditional Granger causality and application to multivariate neural field potential data', Journal of neuroscience methods, 150(2), pp. 228-237, 2006

[95] Zhou, Z., Wang, X., Klahr, N.J., Liu, W., Arias, D., Liu, H., von Deneen, K.M., Wen, Y., Lu, Z., and Xu, D., 'A conditional Granger causality model approach for group analysis in functional magnetic resonance imaging', Magnetic resonance imaging, 29(3), pp. 418-433, 2011

[96] Wang, L., Zhang, J., Zhang, Y., Yan, R., Liu, H., and Qiu, M., 'Conditional granger causality analysis of effective connectivity during motor imagery and motor execution in stroke patients', BioMed Research International, 2016

[97] Mainali, K., Bewick, S., Vecchio-Pagan, B., Karig, D., and Fagan, W.F., 'Detecting interaction networks in the human microbiome with conditional Granger causality', PLoS computational biology, 15(5), pp. e1007037, 2019

[98] Gao, Q., Duan, X., and Chen, H., 'Evaluation of effective connectivity of motor areas during motor imagery and execution using conditional Granger causality', Neuroimage, 54(2), pp. 1280-1288, 2011

[99] Chuang, K.-C., Ramakrishnapillai, S., Bazzano, L., and Carmichael, O.T., 'Deep Stacking Networks for Conditional Nonlinear Granger Causal Modeling of fMRI Data', International Workshop on Machine Learning in Clinical Neuroimaging, pp. 113-124. Springer, Cham, 2021.

[100] Jamaludeen, N., Unnikrishnan, V., Pryss, R., Schobel, J., Schlee, W., and Spiliopoulou, M., 'Circadian conditional granger causalities on ecological momentary assessment data from an mhealth app', IEEE 34th International Symposium on Computer-Based Medical Systems (CBMS), pp. 354-359. IEEE, 2021.

[101] Wada, I., Faizulayev, A., and Bekun, F.V., 'Exploring the role of conventional energy consumption on environmental quality in Brazil: Evidence from cointegration and conditional causality', Gondwana Research, 98, pp. 244-256, 2021

[102] Zhou, Z., Chen, Y., Ding, M., Wright, P., Lu, Z., and Liu, Y., 'Analyzing brain networks with PCA and conditional Granger causality', Human brain mapping, 30(7), pp. 2197-2206, 2009

[103] Liao, W., Mantini, D., Zhang, Z., Pan, Z., Ding, J., Gong, Q., Yang, Y., and Chen, H., 'Evaluating the effective connectivity of resting state networks using conditional Granger causality', Biological cybernetics, 102(1), pp. 57-69, 2010

[104] Faes, L., Nollo, G., and Porta, A.: 'Non-uniform multivariate embedding to assess the information transfer in cardiovascular and cardiorespiratory variability series', Computers in biology and medicine, 42(3), pp. 290-297, 2012

[105] Młyńczak, M., and Krysztofiak, H., ‘Discovery of causal paths in cardiorespiratory parameters: a time-independent approach in elite athletes’, Frontiers in physiology, 9, pp. 1455, 2018

[106] Jaimes-Albarracin, A.D., Orjuela-Cañón, Á.D., Jutinico, A.L., Bazurto, M.A., and Dueñas, E., ‘Brain and heart physiological networks analysis employing neural networks granger causality’, 10th International IEEE/EMBS Conference on Neural Engineering (NER), pp. 469-472. IEEE, 2021.

[107] Corbier, C., Chouchou, F., Roche, F., Barthélémy, J.C., and Pichot, V., ‘Causal analyses to study autonomic regulation during acute head-out water immersion, head-down tilt and supine position’, Experimental Physiology, 105(8), pp. 1216-1222, 2020

[108] Rosoł, M., Młyńczak, M., and Cybulski, G., ‘Granger causality test with nonlinear neural-network-based methods: Python package and simulation study’, Computer Methods and Programs in Biomedicine, 216, pp. 106669, 2022

[109] Greville, W.J., and Buehner, M.J., ‘Temporal predictability facilitates causal learning’, Journal of Experimental Psychology: General, 139(4), pp. 756, 2010

[110] Greville, W.J., Buehner, M.J., and Johansen, M.K., ‘Causing time: Evaluating causal changes to the when rather than the whether of an outcome’, Memory & Cognition, 48(2), pp. 200-211, 2020

[111] Wasserman, E.A., and Neunaber, D.J., ‘COLLEGE STUDENTS'RESPONDING TO AND RATING OF CONTINGENCY RELATIONS: THE ROLE OF TEMPORAL CONTIGUITY’, Journal of the Experimental Analysis of Behavior, 46(1), pp. 15-35, 1986

[112] Greville, W.J., and Buehner, M.J., ‘The influence of temporal distributions on causal induction from tabular data’, Memory & Cognition, 35(3), pp. 444-453, 2007

[113] Greville, W.J., and Buehner, M.J., ‘Temporal predictability enhances judgements of causality in elemental causal induction from both observation and intervention’, The Quarterly Journal of Experimental Psychology, 69(4), pp. 678-697, 2016

[114] Wen, X., Rangarajan, G., and Ding, M.: 'Multivariate Granger causality: an estimation framework based on factorization of the spectral density matrix', Philosophical Transactions of the Royal Society A: Mathematical, Physical and Engineering Sciences, 371(1997), pp. 20110610, 2013

[115] Eichler, M., and Didelez, V.: 'On Granger causality and the effect of interventions in time series', Lifetime data analysis, 16(1), pp. 3-32, 2010

VITA

Mounika Kasaraneni

Candidate for the Degree of

Doctor of Philosophy

Thesis: ANALYSIS OF SLEEP STAE TRANSITIONS AND NETWORK PHYSIOLOGY OF CONTROL AND SLEEP APNEA SUBJECTS

Major Field: Computer Science

Biographical:

Education:

Completed the requirements for the Doctor of Philosophy in Computer Science at Oklahoma State University, Stillwater, Oklahoma in July 2022.

Completed the requirements for the Master of Science in Computer Science at Texas A&M University-Kingsville, Kingsville, Texas in 2017.

Completed the requirements for the Bachelor of Technology in Electronics and Computer Science at S.R.K Institute of Technology, Vijayawada, Andhra Pradesh, India in 2015.